JGR Solid Earth

RESEARCH ARTICLE
10.1029/2018JB016514

Reservoir Structure and Hydraulic Properties of the Campi Flegrei Geothermal System Inferred by Audiomagnetotelluric, Geochemical, and Seismicity Study

Agata Siniscalchi[1], Simona Tripaldi[1], Gerardo Romano[1], Giovanni Chiodini[2], Luigi Improta[3], Zaccaria Petrillo[4], Luca D'Auria[5,6], Stefano Caliro[4], and Rosario Avino[4]

[1]Dipartimento di Scienze della Terra e Geoambientali, Università degli Studi di Bari ALDO MORO, Bari, Italy, [2]Istituto Nazionale di Geofisica e Vulcanologia, Sezione di Bologna, Bologna, Italy, [3]Istituto Nazionale di Geofisica e Vulcanologia, Sezione Osservatorio Nazionale Terremoti, Roma, Italy, [4]Istituto Nazionale di Geofisica e Vulcanologia, Osservatorio Vesuviano, Naples, Italy, [5]Instituto Volcanológico de Canarias, Tenerife, Spain, [6]Instituto Tecnológico y de Energías Renovables, Tenerife, Spain

Key Points:
- We present new audiomagnetotelluric, geochemical, and seismological observations data collected in the central-eastern sector of Campi Flegrei caldera
- The multidisciplinary analysis provides information on the structure and properties of the hydrothermal reservoir and of the fluid pathways
- Seismic events seem linked to the combined action of tectonic lineaments and fluid interactions between gas/steam reservoir and the outflow zone

Supporting Information:
- Supporting Information S1

Correspondence to:
S. Tripaldi,
simona.tripaldi@uniba.it

Citation:
Siniscalchi, A., Tripaldi, S., Romano, G., Chiodini, G., Improta, L., Petrillo, Z., et al. (2019). Reservoir structure and hydraulic properties of the Campi Flegrei geothermal system inferred by audiomagnetotelluric, geochemical, and seismicity study. *Journal of Geophysical Research: Solid Earth*, *124*, 5336–5356. https://doi.org/10.1029/2018JB016514

Received 11 AUG 2018
Accepted 11 MAY 2019
Accepted article online 17 MAY 2019
Published online 18 JUN 2019

Abstract The Campi Flegrei caldera is a large volcanic complex lying in the Campanian Plain, Southern Italy. During its history the caldera experienced episodes of bradyseism and intense swarm seismicity. The mechanism leading to unrest episodes is still debated, and great efforts are ongoing to improve the knowledge of this structure and its evolution due to the high volcanic risk in such a densely populated area. Here we present a resistivity model from a two-dimensional inversion of audiomagnetotelluric data acquired along an approximately 5.6-km long profile crosscutting the Solfatara-Pisciarelli district and the Agnano plain. The resistivity model shows (1) very low resistivity values confined in the first 500 m of depth both in correspondence of the Solfatara-Pisciarelli districts and the Agnano depression; (2) a resistive plume that extends underneath the Solfatara crater down to 2,000- to 3,000-m depth, and (3) an adjoining relative conductive unit eastward. We discuss the resistivity structures in a multidisciplinary framework integrating inedited geochemical and seismological observations with existing surface geology and subsurface information. The Solfatara-Pisciarelli district and the Agnano plain, both being expression of intense hydrothermal activity, show different characteristics. Below the Solfatara-Pisciarelli area, the shallow conductive zone is interpreted as a faulted clay cap that overlies a highly active vapor-dominated reservoir characterized by a convective mechanism. Conversely, below the Agnano plain, a liquid phase seems to prevail in the reservoir. The spatiotemporal variations of seismicity imply a combined action of preexisting tectonic lineaments and fluid interaction between the gas/steam reservoir and the outflow zone.

1. Introduction

The Campi Flegrei caldera (CFc) underwent two important unrest episodes in the last decades that raised great concerns over a possible volcanic eruption in this densely populated area. The central part of the CFc is presently experiencing unrest (Chiodini et al., 2016) and, in spite of extensive studies, the mechanism leading to recent and ongoing episodes is still debated and attributed either to volcanic unrest or to nonmagmatic, hydrothermal unrest with significant implications on hazard assessment (Rouwet et al., 2014). Much information on the hydrothermal system comes from geochemical monitoring, but a comprehensive definition of its internal structure is still lacking. To this end, an electrical characterization may play an important role since resistivity is a suitable parameter to image fluid paths at depth. Magnetotelluric (MT) modeling is therefore considered one of the most powerful tools to understand a geothermal system, as testified by abundant literature (Munoz, 2014; Spichak & Manzella, 2009, and references therein). In high-enthalpy geothermal systems, like CFc, we expect electrical conductive anomalies associated both to hot fluids circulating in faults or fracture systems and to intense clay alteration product of the hydrothermal circulation. The large number of case histories, supported by laboratory data and by direct comparison of MT resistivity distribution with well logs, allowed for a better understanding of the relative role of the factors affecting resistivity in the geothermal systems.

The two typical, electrical conduction mechanisms in clay-bearing, water-saturated rocks are pore fluid conduction and surface conduction, and both mechanisms are temperature dependent. Surface

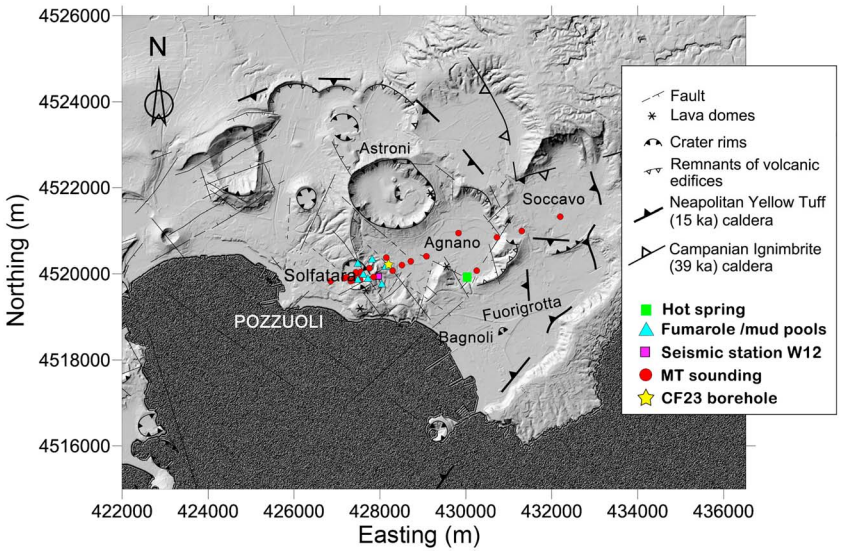

Figure 1. Map of the CFc showing the location of AMT soundings (red dots), geothermal well (star), main fumaroles in the Solfatara-Pisciarelli district (cyan triangles), the Agnano Terme hot spring (green square) and W12 seismometer station. Structures are reported from Di Vito et al., 1999. CFc = Campi Flegrei caldera; AMT = audiomagnetotelluric.

conductivity is directly proportional to the exchange capacity of clays (Ussher et al., 2000) and significantly increases in the temperature range 100–150 °C, while its value decreases at higher temperatures (Komori et al., 2013). Furthermore, as temperature is the major control of clay mineralogy, resistivity distribution can give a rough estimation of temperature inside the geothermal system.

Laboratory data and well logs have shown that, especially in volcanic rock altered by the hydrothermal circulation, clay products are very often the most important factor influencing resistivity of the caprock. However, the presence of clay minerals prevents the application of the classical Archie's law that, in other contexts, allows for a rapid evaluation of fluid amounts, as it states the linearity in log-log scale between conductivity and fluid amounts. In multiphase environments, careful consideration should be made on the type of conductivity enhancement of each anomalous zone and a multidisciplinary approach should be favored. The interpretation of the resistivity anomalies in geothermal areas gains, for example, special benefit from the comparison between cation and gas geochemistry from thermal manifestations. Moreover, both geophysical and geochemical data are among the most relevant surface data to constrain the reservoir properties (Cumming, 2009).

The main aim of this work is to explore the first kilometers of the subsoil of the CFc central-eastern sector in order both to define the deep upraise path of the fluids and to gain insight on the mechanism leading to seismicity during unrest episodes. To this end, we present results from audiomagnetotelluric (AMT) investigation together with new geochemical and seismicity distribution data. Our primary targets are the Solfatara volcano and the nearby Pisciarelli field (see Figure 1), which are experiencing a renewal of hydrothermal activity with increasing flow rates and temperatures, expanding degassing areas and ongoing shallow microseismicity beneath the eastern slope of the crater.

The near-surface Solfatara crater was recently investigated by several authors. Resistivity models, mainly derived through high-resolution electrical resistivity tomography (ERT), are given in Bruno et al. (2007), Byrdina et al. (2014), Isaia et al. (2015), Gresse et al. (2017) for the near-surface Solfatara crater. Troiano et al. (2014) provided a resistivity model resulting by a combined controlled source audiomagnetotelluric (CSAMT) and natural source MT survey along a profile extending from the Solfatara to the Pisciarelli field for a total length of about 1 km.

In this paper we present the results of a multidisciplinary study based on a resistivity image obtained along a 5.6-km-long profile consisting of 22 new and unpublished soundings performed in the framework of the MED-SUV project (see Figure 1). This profile runs WSW-ENE across the central-eastern sector of the

caldera providing new insights into the internal structure of the geothermal system of the Solfatara, Pisciarelli, and Agnano districts down to 3,000 m of depth.

We compare and discuss our new resistivity image with previous published resistivity models and use available geologic and geophysical subsurface data to constrain our interpretation. It will be shown that our results represent a substantial improvement especially regarding the relationship between shallow and deeper resistivity characterization of the geothermal system. The integration of the resistivity model with geochemical records, geophysical data, and earthquake locations provides key information for a better understanding on the structure and properties (i.e., fluid physical state) of the hydrothermal reservoir and of the fluid pathways, as well as on the role played by fluids on the seismicity associated to recent unrest episodes.

2. Geological, Geochemical, and Geophysical Contexts

The CFc is a large volcanic complex hosted in a graben-like structure that lies in the Campanian Plain, Southern Italy (Figure 1). It is characterized by two nested depressions bordered by two concentric segmented caldera rings (Acocella, 2010; Tramelli et al., 2006). The caldera is filled by a 2000- to 3000-m thick sequence of Plio-Quaternary continental and marine sediments and volcanic deposits, the majority of which were deposited during the major eruptions of the Campanian Ignimbrite (about 37–39 ky; Civetta et al., 1997) and Neapolitan Yellow Tuff (about 12 ky; Orsi et al., 1996).

Minor caldera collapses of different size formed between 10 and 5 ky inside the external ring, often following smaller volume eruptions (predominantly phreatomagmatic), as for Agnano-Monte Spina (de Vita et al., 1999). Along the southwestern rim of the Agnano-Monte Spina collapsed area (Figure 1) there are several vents within less than 2 km^2 including the Solfatara volcano (Isaia et al., 2015).

Historical resources and vertical displacement measures allow to reconstruct ground deformation of the central CFc over the last 2,000 years (Parascandola, 1983). After a long phase of slow subsidence initiated in Roman times, the CFc experienced a low-rate ascending phase since the tenth century. This phase was interrupted in the sixteenth century by an episode of rapid ground uplift and intense seismicity (Guidoboni & Ciuccarelli, 2010) that culminated with the last eruption localized in the western sector of the caldera (Monte Nuovo, 1538 A.D.; Figure 1). A new long-term descending phase ended in the late 1960s when the central part of the CFc underwent two episodes of rapid and extended ground uplift (1970 to 1972 and 1982 to 1984) associated to intense seismicity, referenced as *bradyseism crises* (D'Auria et al., 2011). The maximum ground uplift (up to 1.8 m during the 1982–1984 episode) and the location of the earthquakes focused in an area that extends from the town of Pozzuoli to the Solfatara crater. After the last bradyseism episode a ground subsidence started lasting until 2005, when a new inflation initiated, resulting in a minor accelerating uplift (0.4 m over 10 years) of longer duration (Chiodini et al., 2016). Over the last 10 years low-magnitude earthquakes, often clustered in seismic swarm episodes, occurred mainly along the eastern border of the volume involved by the past activity that is the eastern slope of the Solfatara crater. This area of renewed seismic activity includes the Pisciarelli field that hosts a weak phreatic activity where there was the opening of new vents and a significant increase of flow rates and temperatures of existing fumaroles (Chiodini et al., 2016). Long-term geochemical monitoring assess that several kilotons of hydrothermal fluids are emitted daily by the Solfatara-Pisciarelli field through both diffuse soil emissions and vigorous fumarolic vents. From 2003 to 2016, the area affected by the release of deep sourced CO_2 tripled its extent becoming of ~ 1 km^2 and, concurrently, the amount of the diffusively released CO_2 increased up to typical values of persistently degassing active volcanoes (up to 3,000 t/d, Cardellini et al., 2017). Large variations in the H_2O-CO_2–CH_4-CO-H_2-N_2–He-Ar composition of the fumaroles accompanied the increase of the flux of hydrothermal CO_2 (Caliro et al., 2014; Chiodini et al., 2015, 2016).

On the eastern side the hydrothermal activity at the Agnano Terme, in the center of the Agnano crater, is different with respect to the ones in Solfatara-Pisciarelli district because it is characterized by the discharge of thermal waters rather than gas. At Agnano Terme the gas flux and their equilibrium temperatures appear both much lower than at Solfatara (Vaselli et al., 2011).

Correlating seismological, geodetic and geochemical data D'Auria et al. (2011) interpreted the recent dynamics of the CFc as repeated injection of magmatic fluids into the hydrothermal system being the cause of both ground uplift episodes and seismicity. More specifically, Chiodini et al. (2016), based on both the

observed variation at fumaroles (composition and fluxes) and the results of physical simulations, suggest that magma degassing reached a critical pressure implying that increasing amount of magmatic water is injected into the hydrothermal system causing heating and pressurization.

Furthermore, observed ground deformation for the 1982–2013 period would be controlled by pressure changes in two distinct sources: a deeper pressurized triaxial ellipsoid at about 4 km in depth below Pozzuoli and a shallower and smaller pressurized spheroid located at ~2 km in depth below Solfatara crater (Amoruso et al., 2014).

A lot of information on the caldera structure comes from geophysical exploration data as well as from seismological data. Here we will focus mainly on what pertains to the central-eastern sector of the caldera investigated by our AMT survey.

Several deep (2,000–3,000 m) boreholes were drilled onshore for geothermal exploration by AGIP (Rosi & Sbrana, 1987) and SAFEN companies. A recent review of the whole data set is given in Carlino et al. (2012). Among them, only well CF23 is located in the eastern side very close to our profile (see location in Figure 1). This borehole drilled in 1954 (in some papers referenced as Agnano well) has attracted increasing interest being its position close to the Pisciarelli area of increasing hydrothermal activity. Subsurface data indicate a shallower aquifer in the upper 200 m and a deeper one at 1,400-m depth with a temperature of 250 °C (Carlino et al., 2012). Also, a temperature rise to 300 °C (Todesco et al., 2003) and water with a Na plus Cl content of up to 27 g/L (Piochi et al., 2014) were observed at the wellbore (1,800 m below sea level; herein and after bsl). Piochi et al. (2015) reported an argillic sequence (containing abundant clay minerals that formed at the expense of primary feldspar and glass) drilled down to about 750 m (see Figure 8 in Piochi et al., 2015) and underlying a shallow phyllitic zone.

Concerning the deep caldera structure, modeling of offshore seismic reflection data has put in evidence a low-velocity layer about 7,500-m deep and 1,000-m thick that was associated with a partial melting zone beneath the caldera thus considered as the source of the feeding system (Zollo et al., 2008). The present MT investigation, due to its inherent depth of investigation, focuses on a shallow portion of the caldera ascribed to the geothermal reservoir. Reservoir physical properties have been mainly inferred from passive and joint passive-active traveltime seismic tomography (Vanorio et al., 2005 and Battaglia et al., 2008, respectively), as well as from attenuation tomography (de Lorenzo et al., 2001; De Siena et al., 2010). All these tomographic studies are based on the reanalysis of events recorded during the 1982–1984 bradyseismic crisis (Aster & Meyer, 1988).

Vanorio et al. (2005) integrated a reservoir-scale 3D tomography with laboratory measurements and theoretical modeling of physical properties of the CFc rocks to characterize the geothermal reservoirs. Main features of the 3D velocity model, retrieved also by Battaglia et al., 2008, were (i) a very low V_p/V_s flat anomaly at about 4-km depth underneath the center of the caldera interpreted as fractured, gas-bearing formations under supercritical conditions and (ii) a high-V_p/V_s spot at 1.5-km depth just under the town of Pozzuoli interpreted as a brine-saturated zone due to steam condensation. Velocity pattern correlates to earthquake distribution with swarms occurring mostly in the upper part of the low-V_p/V_s zone. We anticipate that the V_p/V_s information reported by Vanorio et al. (2005) provide key constraints to interpret our resistivity image. The 3D tomographic reconstruction of the CFc was further analyzed in Vanorio and Kanitpanyacharoen (2015) to support a rock physics model in which marine basement rocks housing metamorphic decarbonation are covered by an arch-shaped tuffite caprock affected by hydrothermal reactions (depth 1–2 km), overtopping the 1982–1984 seismogenic volume.

De Siena et al. (2010) found high-attenuation vertical structures connected at the surface with the main volcanic structures, fumarole fields, and vertical faults. Underneath the NE sector of the caldera (including the Solfatara area), de Lorenzo et al. (2001) interpreted a low-Qp and low-V_s anomalies as a densely fractured porous medium percolated by fluids, while a deeper low-Qp zone was ascribed to dominant temperature effect on rock rheology.

The shallow structure of the Solfatara crater was the target of numerous high-resolution geophysical surveys based on geoelectrical or active seismic methods (Bruno et al., 2007; Bruno et al., 2017; Byrdina et al., 2014; De Landro et al., 2017; Isaia et al., 2015). In a recent paper, Gresse et al. (2017) presented a 3D ERT of the Solfatara-Pisciarelli district characterized by unprecedented high spatial resolution. The high-resolution

3D resistivity model, integrated with geochemical and temperature data, reveals a two-phase hydrothermal structure and delineates in the near-surface liquid-dominated conductive plumes (< 5 Ω m) underneath the mud pool of Fangaia (hereinafter indicated as FA) and the Pisciarelli fumarole. Also, the high-resolution tomograms identify the fluid pathway feeding the fumaroles of Bocca Grande and Bocca Nuova (hereinafter indicated as BG and BN) as a high-resistivity gas-bearing channel (20–40 Ω m) connecting surface emissions with a gas reservoir at ~ 60-m depth.

Several efforts have been done in order to incorporate geophysical models and geochemical data in a comprehensive model of the geothermal system. Among them Petrillo et al. (2013) developed a 3D physical model of the CFc geothermal system using the TOUGH2 code simulator and taking into account the caldera rocks' physical properties (permeability and porosity empirically derived by density that was obtained from tomographic inversion based on gravity data), bathymetry, and water table topography.

From the wide literature (only partially cited herein), it emerges the big efforts of research put in this area to collect key information for hazard assessment in a so dense populated area. In the assessment of hazard in a volcano-hydrothermal system, like the CFc, the occurrence of hydrothermal nonmagmatic unrest has high probability and in this environment the role of fluids instead of magma as the driving agent could be primary (Rouwet et al., 2014). In this perspective, a multidisciplinary approach integrating MT resistivity modeling, geochemical analyses, and seismological data could be a powerful tool.

3. Material and Methods

3.1. MT Data and Electrical Resistivity Model

The MT method exploits natural electromagnetic (EM) fields to investigate the Earth's subsurface electrical conductivity. AMT refers to recording > 100 Hz to 10 kHz. In the frequency domain, the complex MT impedance tensor Z relates colocated electric (E) and magnetic (H) fields:

$$\begin{bmatrix} E_x(\omega) \\ E_y(\omega) \end{bmatrix} = \begin{bmatrix} Z_{xx}(\omega) & Z_{xy}(\omega) \\ Z_{yx}(\omega) & Z_{yy}(\omega) \end{bmatrix} \begin{bmatrix} H_x(\omega) \\ H_y(\omega) \end{bmatrix} \tag{1}$$

Equation (1) holds assuming that the source fields are homogeneous plane waves. The elements of Z are used to obtain the apparent resistivities and phases:

$$\rho_{ij}^{a}(\omega) = \frac{1}{\mu_0 \omega} \left| Z_{ij}(\omega) \right|^2, \phi_{ij}(\omega) = \tan^{-1} \left[{}^{\mathrm{Im}\left(Z_{ij}(\omega)\right)} \Big/ {}_{\mathrm{Re}\left(Z_{ij}(\omega)\right)} \right] \tag{2}$$

For basic principles of the method and its practical applications, a detailed explanation may be found in Simpson and Bahr (2005) and Chave and Jones (2012).

As a part of the MED-SUV project, the AMT survey was carried out in the period 2012–2014 with a Stratagem EH4 system. As the first recordings revealed the prevalence of low-resistivity values it soon became obvious the necessity to extend the impedance estimation with respect to the classical AMT range to better investigate geothermal targets. With this aim, the acquisition system was equipped also with the low-frequency extension, thus using two different sets of sensors for the electric (two dipoles) and magnetic horizontal components to record data in the frequency range 0.1–10^5 Hz. To improve signal-to-noise ratio, a controlled source in the frequency range from 1,000 Hz to 64,000 Hz was used for low quality data (further technical information is presented in the supporting information). During the project, at each successive measurement campaign, we made repeated site measurements to control stability of the AMT response. Data quality was generally high, particularly for sites located inside the Solfatara crater, where several soundings were acquired at least twice from 2012 to 2014. These repeated soundings showed seasonal variations in AMT experimental curves outside the Fangaia mud pool, while soundings performed inside Fangaia mud pool did not show significant changes (supporting information Figure S1). Whatever the origin of this effect (e.g., see Romano et al., 2014), we selected only soundings performed in the autumn-winter period in order to prevent the introduction of seasonal near-surface distortions in the inversion procedure.

The selected data set consists of 22 soundings (Figure 1) along a profile crosscutting the Solfatara-Pisciarelli-Agnano area. Site distribution is less dense in the eastern area due to logistic difficulties.

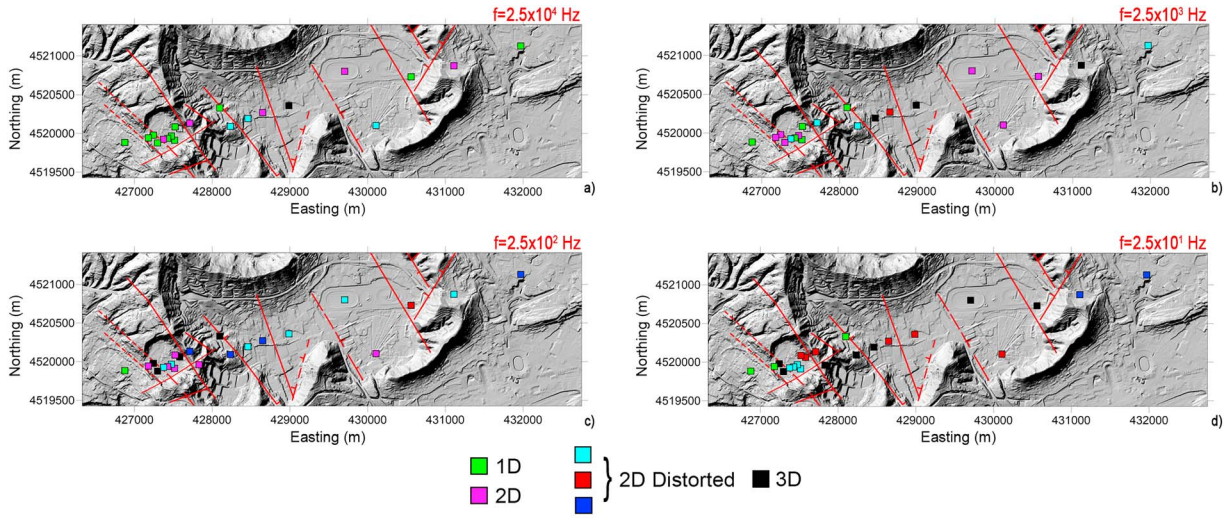

Figure 2. Dimensionality analysis at four frequencies performed applying Weaver's criteria. The cyan, red, and blue 2D distorted cases represent, respectively, galvanic distortion over a 1D or 2D structure, 2D affected by galvanic distortion, and general case of galvanic distortion over a 2D structure.

As the geoelectric directionality and dimensionality of the data can be explored with different sets of rotational invariants associated to the impedance tensor, we first applied Weaver's criteria on rotational invariants (Weaver et al., 2000) including data errors and threshold values (Martí et al., 2004) to determine data dimensionality, to highlight the presence of galvanic distortions, and to estimate the variations of the geoelectric strike in a prevailing 2D assumption as a function of the investigated depth. Inside the highest frequency range (10^3–10^5 Hz) the geoelectric dimensionality is mostly 1D or 2D (Figures 2a and 2b), while at lower frequencies 2D galvanic distortion and even 3D cases increase (Figures 2c and 2d).

This could be ascribed to complexity increase and/or to inductive sea effect even if the latter should be expected at the lowest frequency range since (i) the thickness of the water layer reaches 100 m at a distance of about 5 km from the sounding closest to the coast and (ii) the study area is characterized by low resistivities, thus a moderate conductivity contrast exists between inland and sea. Since the dimensionality analysis is fundamental to evaluate applicability of 2D inversion schemes, we also performed the phase tensor analysis (Caldwell et al., 2004). In agreement with results obtained applying Weaver's analysis, phase tensor ellipses are mainly of circular shape at high frequencies (supporting information Figure S2), suggesting that 1D condition is met in the shallow conductivity structure. At lower frequencies the phase tensor ellipses suggest the presence of higher dimensionality conditions that is better investigated studying the distribution of β, the skew angle that is a measure of the tensor's asymmetry (Caldwell et al., 2004). This parameter should be comprised in the range $\pm$ 3° to consider the quasi-2D interpretation valid, and it would be advisable not to exceed this threshold (Booker, 2014; Caldwell et al., 2004). In our data set, β values almost completely fall within the recommended limits at the two highest frequency bands (Figure 3). At lower-frequency bands an increased number of β values exceeds these limits, although most of the values fall within the range $\pm$ 5° (Figure 3), a threshold not too inflated if we consider less conservative cases already reported in the reviewed literature (Booker, 2014).

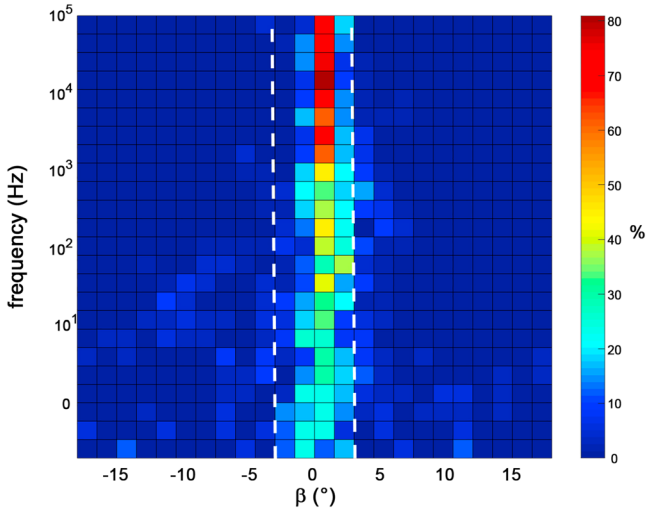

Figure 3. Percentage occurrences of the skew angles β calculated within logarithmically equally spaced bin. The two dashed lines represent the range $\pm$ 3°.

Summing up, the dimensionality analysis showed the presence of cases that deviate from 2D. High skew values (i.e., $\beta > 5°$) are mainly found for frequencies lower than 100 Hz and particularly for the easternmost soundings along the profile (Figure S2). Thus, we expect that the 2D resistivity modeling would not be able to correctly retrieve all the deep and easternmost resistivity features. Less constrained regions of the model may change with a 3D inversion approach. However, 3D modeling of

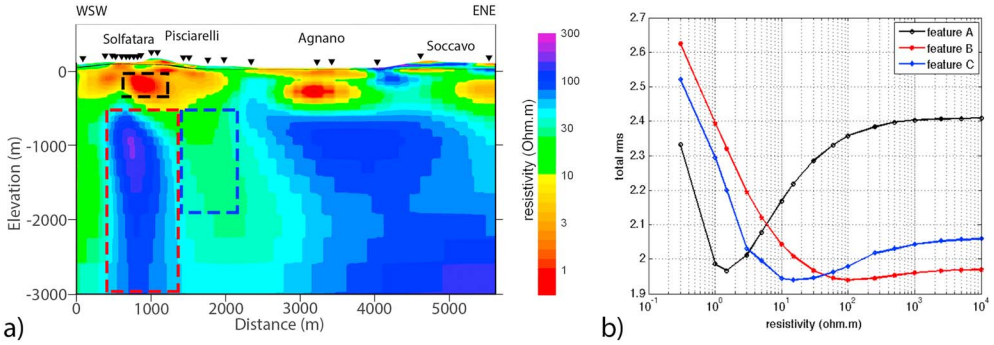

Figure 4. (a) Two-dimensional resistivity inversion model: black triangles on top represent the AMT stations. (b) Sensitivity analysis results: each colored line corresponds to the RMS misfit calculated by varying over several orders of magnitude the resistivity values in the corresponding colored dashed box in Figure 4a. RMS = root-mean-square; AMT = audiomagnetotelluric.

data acquired in 2D geometry (profiles) cannot ensure to achieve a more reliable result. Indeed, 3D modeling outcomes may be affected by distortion and results may vary also depending on the completeness of the data set (Miensopust et al., 2013). According to many authors, when the 2D assumption is reasonable and the data are properly undistorted, first-order structures obtained from 2D inversion are in good agreement with those obtained from 3D inversion (i.e., Tietze & Ritter, 2013, and herein references). Since the 2D approach can still be considered reasonable and valuable under the discussed conditions, the data set was prepared for 2D inversion.

When data dimensionality justifies the use of the 2D assumption, the recovered strike angle in the lowest frequency band (0.2-10^2 Hz) is confined around N30°W (supporting information Figure S3). Directionality analysis suffers from 90° ambiguity; however, the recovered strike angle is almost consistent to the outer caldera major axis (Acocella, 2010) and to the direction of the main faults (Figure 2) in the surveyed area, which strike is predominantly NW-SE.

Hence, the data were corrected for distortion using the procedure described in Weaver et al. (2000) and rotated into the transverse electric mode (TE, currents flowing parallel to the strike direction) and the transverse magnetic mode (TM, currents flowing perpendicular to the strike direction) along the N30°W strike direction and smoothed considering the consistency between resistivity and phase with the D+ technique (Beamish & Travassos, 1992).

After applying the undistortion procedure, some apparent resistivity estimates derived from the impedance tensor diagonal elements assume high magnitude (Figure S5), confirming the 3D character of the data already revealed by the dimensionality analysis (Figure S2).

The obtained data set was inverted using the nonlinear conjugate 2D inversion algorithm of Rodi and Mackie (2001). The inversion problem is solved seeking a model that minimizes a regularized objective function (Tikhonov & Arsenin, 1977) that is a combination of roughness and data misfit.

The code can invert the conventional polarization modes (TE and TM) separately or jointly (TETM).

The TM and TE modes satisfy the principle of information complementarity (Berdichevsky, 1999), thus, bimodal (TETM) 2D inversions are routinely undertaken. Nevertheless, since the 2D modeling of 3D data may introduce questionable features in the models (Ledo, 2005), individual modes (TE and TM) were also run to compare key features. To explore the model space, a number of inversions were carried out using different values of the algorithm parameters.

The preferred resistivity model (Figure 4a) has been obtained inverting both TE and TM modes and using a two layers starting model below the surveyed area (a 10 Ω·m resistivity layer up to ~3,000 m overlying a homogenous half space of 100 Ω·m) and includes topography and a simplified sea layer fixed at 0.3 Ω·m toward WSW.

The variable that controls the amount of regularization (τ, smoothing) was set to 5 by considering the trade-off between root-mean-square (RMS) and roughness (supporting information Figure S4), while the assigned

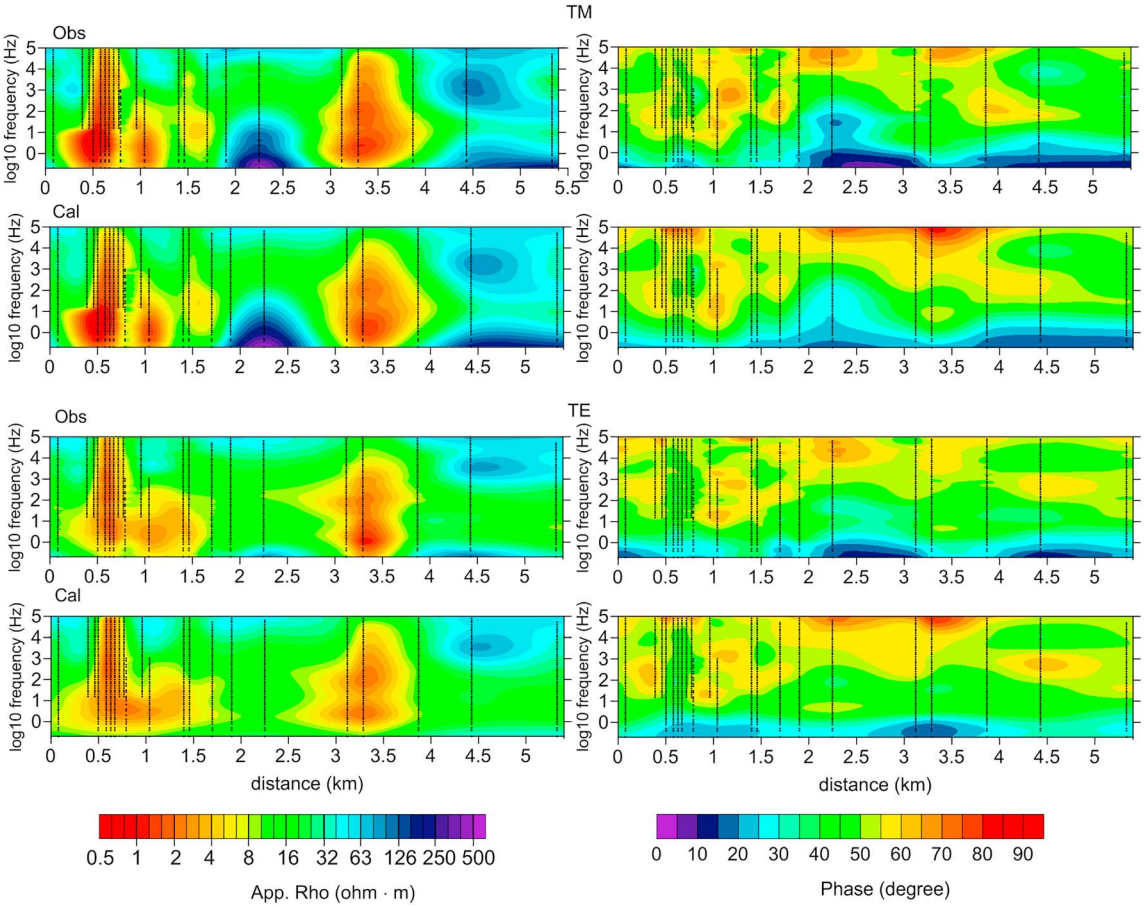

Figure 5. Pseudosections for the observed (OBS) and calculated (CAL) data along the AMT profile. AMT = audiomagnetotelluric.

error floors to the apparent resistivities and phases were 14% and 6%, respectively. Using these settings, the normalized RMS misfit weighted for the given error floors is 1.93.

Generally, putting greater weight on fitting the phase should better accommodate the data for static shift effects (Ogawa, 2002), and independent resistivity measurements may provide a valuable cross check control (i.e., Àrnason et al., 2010; Sternberg et al., 1988; Tripaldi et al., 2010). The presented resistivity model was obtained with a slight increase in weight on the phase data; however, the shallower part (<250 m) within the Solfatara area (supporting information Figure S7) agrees very well with the DC resistivity models of Byrdina et al. (2014) and Gresse et al. (2017). This comparison, although qualitative, suggests that static and topographic effects do not influence significantly our AMT data, at least in the compared area.

Both observed and calculated apparent resistivity and phase data for the TE and TM mode are shown in Figure 5 (data fit curves of all soundings are in the supporting information, Figure S5). The fit of TE mode appears slightly worse than TM one, maybe because of 3D effects at longer periods. To what extent the use of the TM mode inversion is more appropriate than the TETM one, in the presence of 3D structures, is a long-lasting issue. As a general rule, it should be borne in mind that the effectiveness of different inversion modalities depends on the geological context (i.e., Berdichevsky, 1999; Jones, 1983; Wannamaker et al., 1984).

As expected, the resistivity image obtained from TM inversion (supporting information Figure S6) exhibits some differences with respect to the TETM one, but the most significant anomalies are generally consistent. Thus, despite the larger data misfit the joint TETM inversion was preferred also because of the good consistency with independent data (section 4).

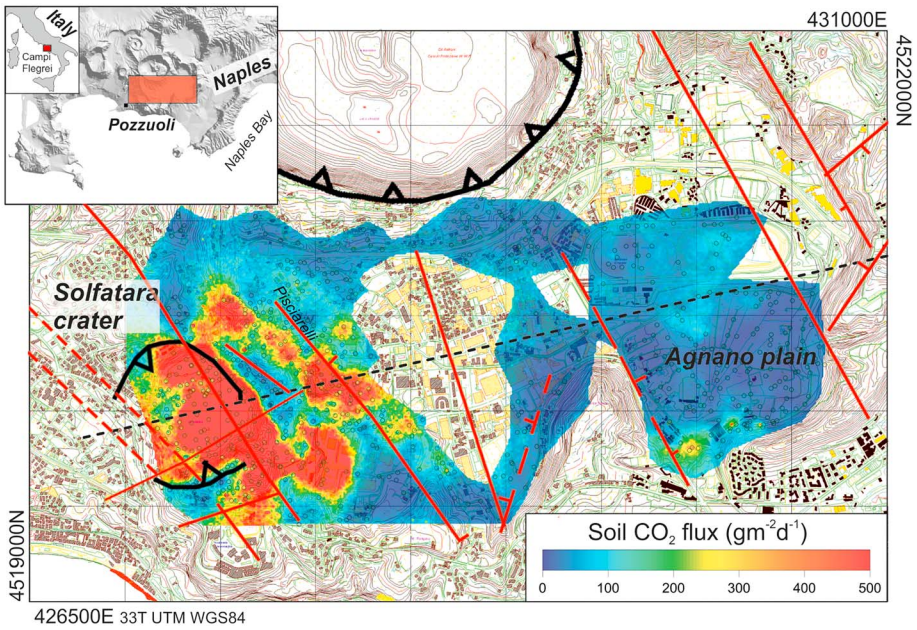

Figure 6. Soil diffuse CO_2 degassing at Solfatara crater and Agnano plain in the spring 2006 overlaid on the regional technical map, 1:5000 Regione Campania. The main caldera structures and faults are redrawn after Isaia et al., 2015; Piochi et al., 2015; Vilardo et al., 2010.

Since the imaged features are critical to characterize the geothermal reservoir and to understand the feeding system of the Solfatara-Pisciarelli emissions, we tested the robustness of three zones of the resistivity model by performing a nonlinear sensitivity test (Nolasco et al., 1998): (i) the conductive area connecting Solfatara and Pisciarelli in the depth range 150–350 m bsl (feature A, black dashed rectangle in Figure 4a); (ii) the resistive plume above the eastern side of Solfatara (feature B, red dashed rectangle in Figure 4a); and (iii) the adjoin conductive area (feature C, blue dashed rectangle in Figure 4a). Solving the forward problem in each zone for different resistivity values ranging over several orders of magnitude, we analyzed the total RMS misfit as a function of the resistivity (Figure 4b). In all the cases the curves show a minimum, which represents the optimal resistivity values in terms of fitting, whose values are 1.5 Ω·m (feature A), 120 Ω·m (feature B), and 15 Ω·m (feature C). It should be noted that feature A appears well constrained on both sides of the minimum, whereas for the other two features the RMS value increases notably for resistivity values lower than the optimal ones and the RMS increases smoothly for higher resistivity values. These results suggest that the two features are better constrained in their lower resistivity boundary. For the upper resistivity boundary the feature C is better constrained than feature B, but the smooth general trends could be due to the general resistivity increase at depth greater than 3,000 m, as suggested by phases behavior at lowest frequencies (Figure 5).

3.2. CO_2 Flux Data

The used data set (total 740 points) consists of published and unpublished data (403 and 337, respectively) of soil diffuse CO_2 flux measured in the spring 2006 over an area that roughly includes the Solfatara crater and the Agnano plain (Figure 6).

The data acquired at Solfatara, 403 measurements, were already published in a specific work together with the data of other 29 diffuse CO_2 flux surveys performed in the same area from 1998 to 2016 (Cardellini et al., 2017). According to Cardellini et al. (2017), in the spring 2006 Solfatara crater emitted 1,242 ± 135 tons per day of CO_2 by soil diffuse degassing.

The other 337 measurements were performed in order to expand the surveyed area of Solfatara toward east including the crater of Agnano and are here used for the first time. The flux was measured with the accumulation chamber method (Chiodini et al., 1996, 1998), which is based on the continuous detection of the CO_2 concentration inside a small chamber placed on the ground. Briefly, the CO_2 flux is proportional to the time

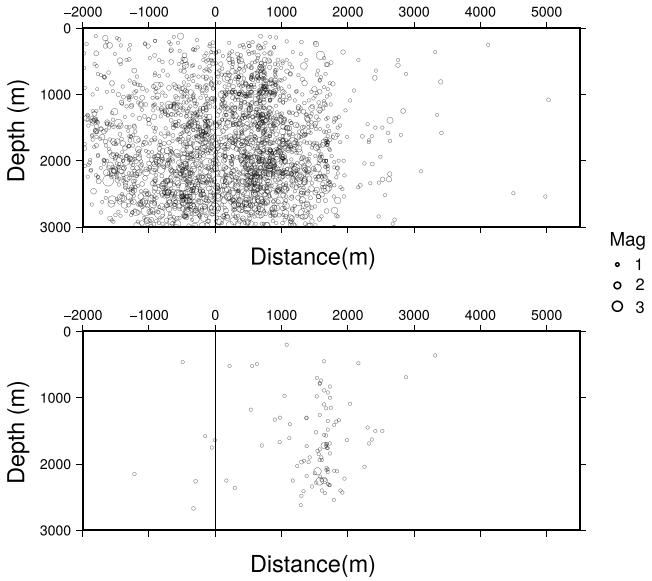

Figure 7. Earthquakes located along the direction of the AMT profile (within ±0.5 km) occurred during the 1982–1984 crisis (at top) and during 2005–2016 (bottom). AMT = audiomagnetotelluric.

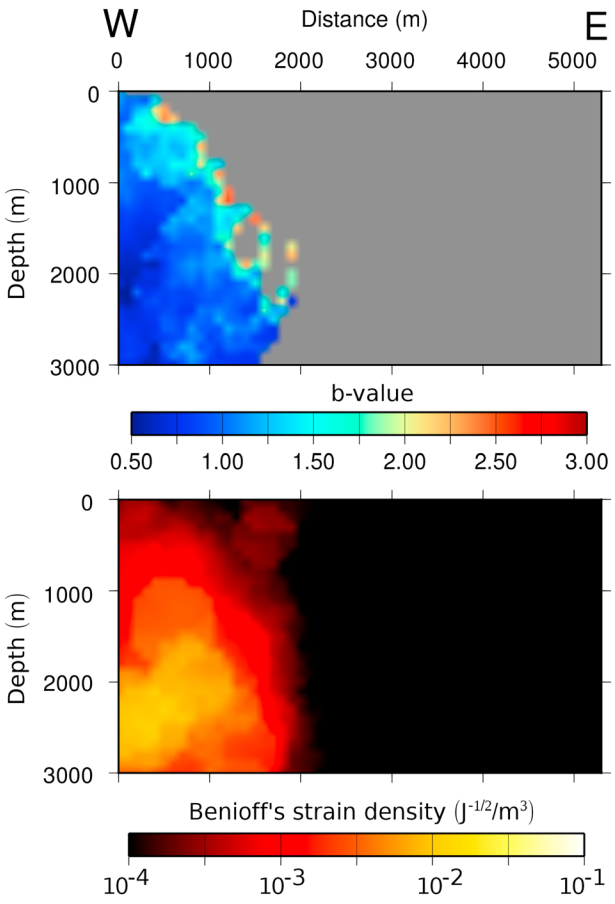

Figure 8. Maps of the *b* value (top) and Benioff's strain release (bottom) along the AMT profile. AMT = audiomagnetotelluric.

derivative of the gas concentration during the first minutes of the measurement. The used instruments were set up, and calibrated regularly before each survey, at the INGV-Napoli laboratories. The errors of calibrated instruments are typically of 10% (Chiodini et al., 1998). For further details on the method we remand to the Cardellini et al. (2017) paper.

The data were used to make the map of CO_2 flux (Figure 6) resulting from 200 simulations performed using the sGs algorithm (sequential Gaussian simulation, Cardellini et al., 2003; Deutsch & Journel, 1998). The map reports for each location the average soil CO_2 flux of the 200 simulations. The line A-A1 (black dashed line in Figure 6) indicates the trace of the CO_2 flux section that, in the following, is used for a comparison with the AMT section.

3.3. Seismicity

The study of microseismicity has shown to be an extremely useful tool for the spatial mapping of the physical properties of hydrothermal reservoirs and their dynamical properties (Kaven et al., 2014). Seismicity in volcanic areas is closely related to the presence of fluids, to the rheology of the crust, and to the local and regional stress fields. In particular, it has been observed that, in some geothermal systems, seismic activity tends to occur at the edges rather than within the production zone (Majer & McEvilly, 1979).

We used the earthquake data set of D'Auria et al. (2011), consisting of about 17,000 earthquake locations recorded between 1983 and 2010 in the CFc (Figure 7). We added to this data set about 700 more events for the interval 2011–2016, from the catalog of Osservatorio Vesuviano-Istituto Nazionale di Geofisica e Vulcanologia. To quantify the seismicity, we computed the Benioff's strain release density (Benioff, 1951) mapping its spatial distribution along the AMT profile using an averaging window with a radius of 500 m.

Another important quantity to characterize the seismicity in volcanic areas is the Gutenberg-Richter *b* value. It is usually close to 1.0 but, in volcanic areas, the presence of fluids often increases this value (Farrel et al., 2009). On the other hand, D'Auria et al. (2011) reported for the CFc *b* values that tend to be lower than 1.0 (D'Auria et al., 2011). A possible explanation of this is the presence of highly fractured rocks and/or high-stress regimes (Farrel et al., 2009). We have computed the *b* value along the AMT profile using for each point of a regular grid, all the earthquakes located within a radius of 500 m from it, applying the maximum-likelihood formulation of Ogata and Katsura (1993). The value was computed only where at least 50 earthquakes were available.

We computed both the Benioff's strain release density and the *b* value only for the 1983–1984 data set (Figure 8, lower and upper panel, respectively), as the number of events was too scarce in the following period to perform these analyses. For the 2005–2016 data set, it was only possible to compute an overall *b* value of 0.92 ± 0.11; this value has to be compared with the 1983–1984 data set of 0.69 ± 0.2 (García-Hernández et al., 2018, see supporting information Figure S10).

The general distribution of the 1983–1984 seismicity is highly asymmetric compared to the observed ground deformation pattern, which is more concentrated in the Solfatara area, to the east of the maximum of the vertical ground displacement observed in the Pozzuoli area (D'Auria et al., 2011; De Siena et al., 2017). In Figure 8 we observe that the highest values

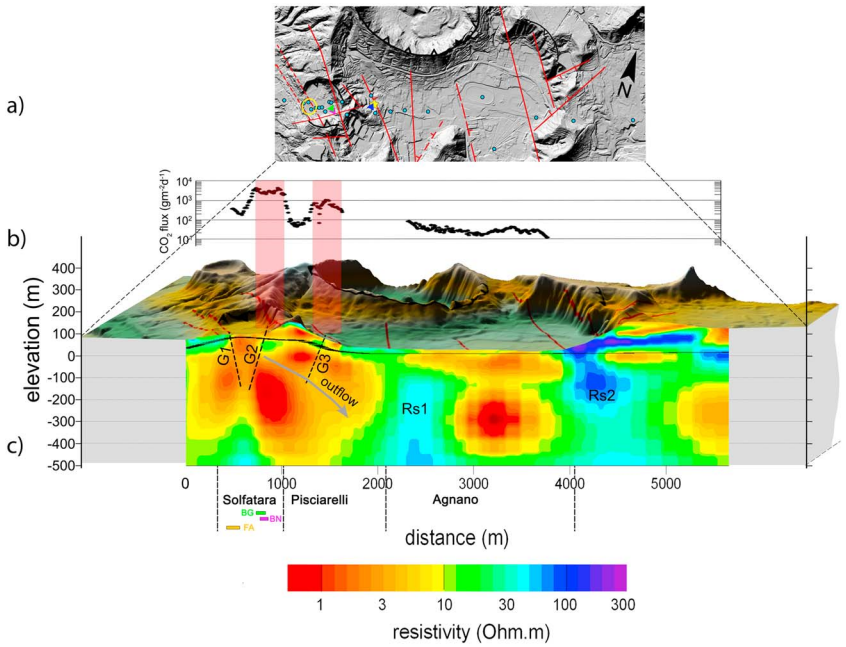

Figure 9. Comparison between the shallow portion of the resistivity model and independent data. (a) Map of the main caldera structures and faults (redrawn after Isaia et al., 2015; Piochi et al., 2015; Vilardo et al., 2010); red lines represent the faults already reported in Figure 1; green, violet, and blue triangles, respectively, represent the BG, BN, and Pisciarelli fumaroles; yellow circle represents the Fangaia mud pool; the yellow star represents the CF23 borehole. (b) CO_2 flux measured along the AMT profile (red shaded boxes highlight the spatial correspondence between geochemical and resistivity data, marking zones of high CO_2 flux and degassing vents). (c) Shallow resistivity distribution (vertical exaggeration 2:1) and the water table level; the structures reported in Figure 9c are the same shown in Figure 9a. Labels G1–G3 in Figure 9c are gaps in the clay cap due to fracture zones as discussed in the text. Note that Figures 9b and 9c are not in scale with Figure 9a. Topography data were extracted from DEM, Regione Campania. AMT = audiomagnetotelluric.

of the Benioff's strain release are located just beneath Solfatara, at depths between 2 and 3 km. The corresponding map of the *b* value shows low values under the Solfatara crater and higher going toward E.

These observations suggest that, during the 1983–1984, seismicity was driven not only by the high-stress regime induced by the active ground uplift source, but clearly hints on a pivotal role of the hydrothermal system in generating the seismicity of CFc. It is relevant to observe that most earthquakes that occurred during the 2005–2016 period are shifted to the east with respect to the 1983–1984 seismicity. As shown by Chiodini et al. (2015), since 2005 there was a striking correlation between geochemical observables, ground deformation, and seismicity in the CFc, pointing to a causative relationship between the dynamics of the hydrothermal system and geophysical unrest. Notably, the seismicity rate appears to be strongly modulated by fluid injection episodes in the hydrothermal system. The only exception is the 2012–2013 rapid uplift episode, which was interpreted by D'Auria et al. (2015) as a small magmatic intrusion, which had only a minor effect on the seismicity of the CFc.

4. Comparison of AMT Resistivity Model With Other Geological and Geophysical Data

The 2D resistivity model (Figure 4a) is characterized by a quite narrow resistivity range (1–300 Ω·m) that well matches the typical range of volcano-hosted geothermal systems (Johnston et al., 1992; Ussher et al., 2000). The surveyed area is densely monitored and widely surveyed enabling us to provide a constrained and integrated interpretation of the resistivity model by using independent data acquired close to our profile. Observing that the lower resistivity values are confined in the first 500 m bsl, we first describe and interpret this shallow portion of the model (Figure 9) and then the deeper one (Figure 10), each time comparing our results with independent observations that are related to the same depth ranges.

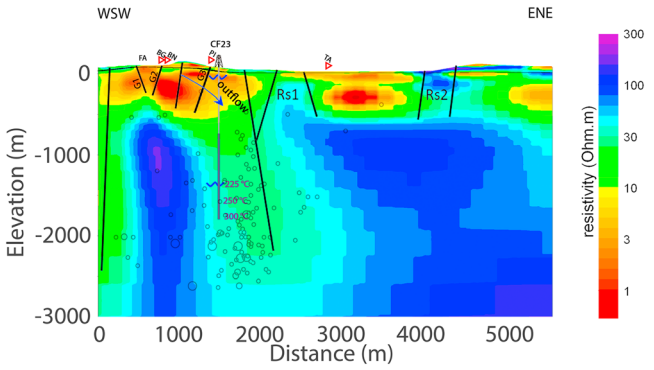

Figure 10. Resistivity model and overlaid: (i) a synthesis of well CF23 stratigraphy (light gray and dark gray represent the Argillic and Phyllitic zones, respectively) and the depth of the two aquifers are represented by blue wavy lines (Piochi et al., 2015); (ii) temperature values measured in CF23 (Todesco et al., 2003); (iii) WTL (Petrillo et al., 2013 and reference therein); (iv) the interpreted faults; and (v) the 2005–2016 seismicity represented by circles whose radius corresponds to magnitude (see Figure 7). WTL = water table level.

4.1. Shallow Portion of the Model

The shallow resistivity distribution (down to 500 m bsl, Figure 9c) is compared to geological and geochemical data (Figures 9a and 9b). The main caldera structures and faults are redrawn from literature (Isaia et al., 2015; Piochi et al., 2015; Vilardo et al., 2010, Figure 9a).

The near-surface resistivity contrasts correlate well with the exposed volcanic structures. Two high-resistivity shallow zones, Rs1 and Rs2 (Figure 9c), correspond to the southern and eastern rims of the Agnano-Monte Spina crater, respectively. Very low resistivity values (< 5 Ω·m) are found both in correspondence of the Solfatara-Pisciarelli districts and the Agnano depression. The water table level lies, almost everywhere, within zones of resistivity values in the range 5–10 Ω·m, thus indicating a significant freshwater supply.

Focusing on the Solfatara volcano, the near-surface is characterized by a very conductive zone (< 3 Ω·m) under the center of the crater that matches the water upwelling of the FA mud pool and merges at depth into a wide conductive region 300- to 400-m thick.

Conversely, a resistive spot (10–20 Ω·m) localized under the eastern margin of Solfatara correlates strongly with the fumaroles of BG and BN (green and magenta triangles in Figure 9a). The bottom of this resistive feature is delimited by a wide conductive zone at a few tens of meters depth (bsl) and seems to extend laterally underneath the eastern flank of the crater. Such resistivity distribution points to a two-phase hydrothermal system in the near-surface with adjacent water-saturated (caused by steam condensation) and vapor-bearing zones (i.e., BG and BN emissions). This observation agrees with previous interpretations of higher-resolution shallow ERT (Byrdina et al., 2014; Gresse et al., 2017) and suggests a shallow origin of the gas-dominated reservoir feeding the fumaroles.

Below sea level a wide conductive zone (as low as 1–3 Ω·m) characterizes the subsurface underneath Solfatara-Pisciarelli (S-P) district. The top of this zone with the same extension and resistivity values was also imaged by ERT survey (Figure 7 in Gresse et al., 2017), while a previous AMT model did not reveal its presence elsewhere (see Figures 6 and 7 in Troiano et al., 2014).

The resistivity value characterizing this high-conductive zone may be ascribed to surface conductivity mechanisms connected to clay minerals produced by hydrothermal fluid alteration. This interpretation is supported by (i) the presence of an argillitic sequence containing abundant clay minerals, extending from surface to about 750 m, in the CF23 well (Piochi et al., 2015); (ii) resistivity laboratory measurements made both on the CFc surface and core samples from deep Agip wells that have shown a strong increase in effective conductivity only in the presence of fluid-activated surface conductivity (Giberti et al., 2006).

Assuming the resistivity structure as a *maximum thermometer* because the alteration is generally unaffected by subsequent cooling (Àrnason et al., 2010), the wide, high-conductive zone can be interpreted as a hydrothermally mineralized clay-rich caprock where temperature does not exceed 150–200 °C. Indeed, at a temperature greater than 200–240 °C, the ions associated to the alteration products are bound in the crystal lattice and are, therefore, more resistive. Saline fluids could further contribute to locally enhance conductivities (Flóvenz et al., 2005).

The lateral continuity of the very low resistivity zone seems to be interrupted by three less conductive subvertical zones (Figure 9c). The first, almost vertical one (G1), is found underneath the FA mud pool. The other two are located just below the highly degassing vents both in the eastern Solfatara and in the Pisciarelli area (G2 and G3, respectively) where diffuse CO_2 flux increase (Figures 6 and 9). We interpret such gaps in the clay cap as due to fracture zones within which pressurized gas escapes from a deeper reservoir as observed in other geothermal system (Rodriguez et al., 2015). This interpretation is supported by two lines of observations: (i) gas emissions correlate to NW-SE trending fault/fracture systems crossing the eastern side of the Solfatara crater and the Pisciarelli area (Cardellini et al., 2017; Isaia et al., 2015); (ii) the presence of subvertical faults disrupting the crater volcanoclastic filling inferred down to 200–300 m bsl by seismic reflection shallow profiles (Bruno et al., 2017).

A further interruption in the conductive zone, whose dip follows the surface topography, might represent the main outflow meteoric path since it mimics the typical asymmetric shape of the clay cap in a steep terrain (Anderson et al., 2000). Here an outflow, mainly of meteoric origin, is documented even in the geochemical record. Indeed, in the Pisciarelli fumarole output an annual cycle of CO_2 contents indicates the occurrence of shallow secondary processes that mask the deep geochemical signals (Chiodini et al., 2011). In addition, Caliro et al. (2007) stated that most of the H_2O is of meteoric origin in the Pisciarelli sites.

Eastward, the high-resistivity structures Rs1 and Rs2 bound the Agnano depression, whose resistive bottom lies at about 500 m bsl (Figure 9c). The whole resistivity structure depicts clearly the collapsed area. Assuming a thickness of 500 m and a diameter of 1,500 m, a rough estimation of the volume returns a value ≈ 0.9 km^3. This volume is compatible with previously estimated erupted products of 1.2 km^3 (de Vita et al., 1999). This collapsed area is filled with conductive material, although at about 180 m bsl the slight resistivity increase could indicate the presence of a shallow freshwater aquifer as also encountered in the CF23 borehole. The long-term geothermal activity in this area supports the same interpretation of the low-resistivities as due to an argillic alteration sequence.

4.2. Deeper Portion of the Model

The most noticeable feature of the deeper resistivity section is a resistive plume-like body centered under the Solfatara and bounded to the east by a relative conductive unit (10–30 Ω·m, Figure 10).

The top plume is at a depth of about 500 m bsl in correspondence of a thinning of the clay layer whose bottom climbs up to 300 m bsl probably reflecting the occurrence of more resistive minerals (i.e., illite), which are typical products generated at higher temperatures in the mixed layer (i.e., depth; Munoz, 2014). Its geometry depicts reasonably the main upflow zone of Solfatara-Piciarelli hydrothermal system.

In this part of the profile and in the same depth range, a partial agreement between the presented MT model (Figure 10) and the one shown in Troiano et al. (2014) can be established (see also Figure S8). The model of Troiano et al. (2014) also displays a plume-like resistive body (50–100 Ω·m) and an adjacent conductive zone to the east. However, the plume-like resistive body of Troiano et al. (2014) reaches the near-surface and merges at about 2,250-m depth into a higher resistivity plate-like body, which extends westward up to the model edge. In addition, the adjacent conductive zone is confined between a depth of 1,200 and 3,000 m along the eastern edge of the section and has considerably lower resistivity values (down to 1–2 Ω·m). Such discrepancies in terms of lateral and shallow features of the two MT models might be ascribed to the different lateral extension of the profiles: that of Troiano et al. (2014) spans only for about 1 km from the inner part of Solfatara to the Pisciarelli field. The MT method suffers from inductive effects of bodies outside the surveyed area and our 5-km-long profile, extending significantly beyond the Solfatara-Pisciarelli district, is expected to better define lateral resistivity contrasts.

In partial agreement with Troiano et al. (2014), we interpret the plume-like resistive body as determined by a higher-temperature fractured propylitic alteration with steam/gas filling the fractures within the hydrothermal system that develops just under the Solfatara crater. Furthermore, in this study we have inferred the presence of a clay-rich cap (i.e., the very conductive zone) topping the gas-bearing resistive plume.

4.3. Comparison With Passive Seismic Tomography

Interpretation of the deep portion of our resistivity model is aided by the reservoir-scale local earthquake tomography (LET) of Vanorio et al. (2005). LET is commonly employed in geothermal fields (Husen et al., 2004, among others) and enhanced geothermal experiments (Calò & Dorbath, 2013; Julian et al., 2010, among others) because it can provide information on the geometric and petrophysical properties of reservoirs that are complementary to those obtained by other geophysical tools, as MT surveying. Different from the *S* wave, the *P* wave velocity in porous or fractured rocks is very sensitive to the physical state of the medium, and consequently, the V_p/V_s ratio can give insights into pore fluid state and pressure (Wang & Nur, 1989). In hydrothermal reservoirs, very low V_p and low V_p/V_s can indicate gas-bearing pressurized formations (i.e., steam), whereas intermediate V_p and high V_p/V_s are diagnostic of liquid-bearing formations (i.e., brine-saturated zones due to steam condensation).

Even though the velocity model of Vanorio et al. (2005) is characterized by a very high spatial resolution for a LET inversion (i.e., 500 m), the V_p and V_s tomographic images could not resolve the small-scale shallow

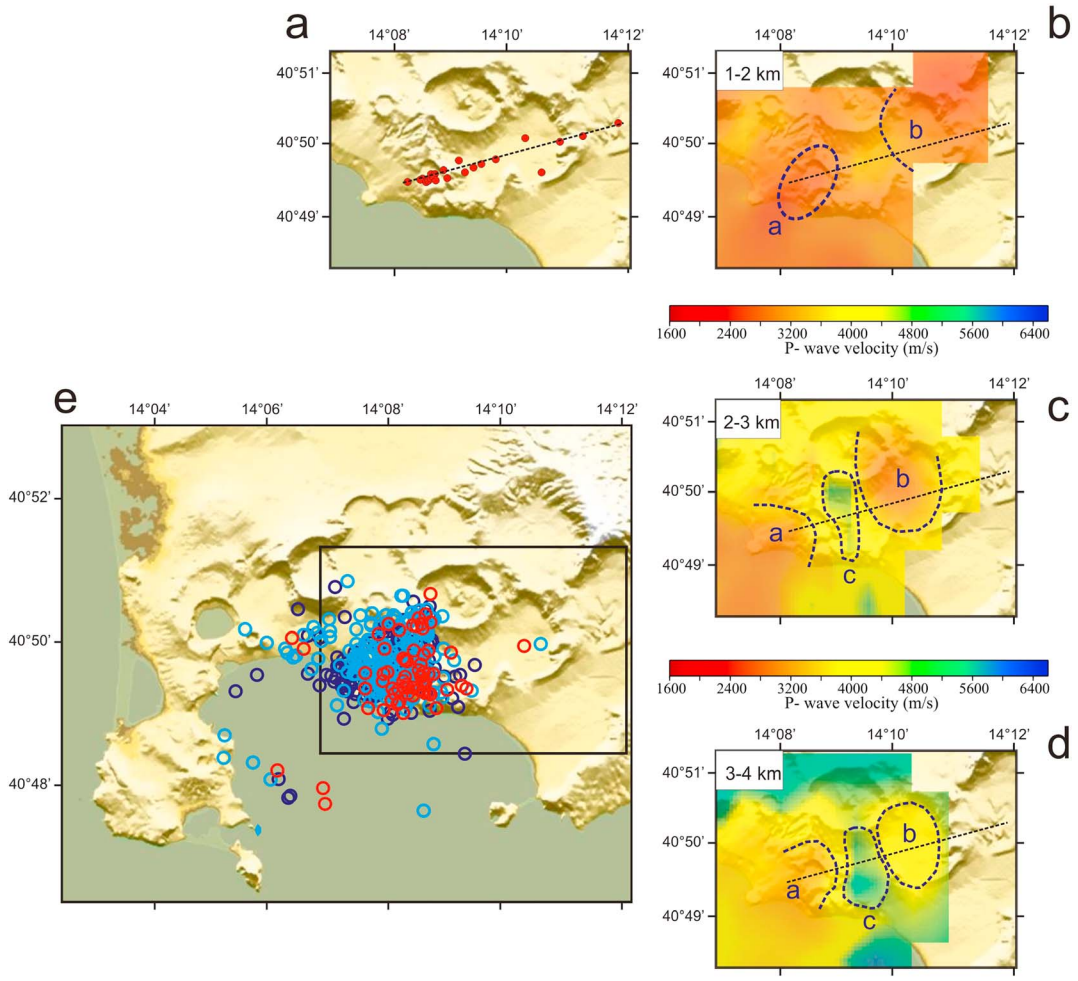

Figure 11. The *P* wave velocity structure in the study area as defined by the Local Earthquake Tomography (modified from Vanorio et al., 2005). (a) Location of AMT soundings (red dots). The AMT profile is depicted with a dashed line. (b to d) V_p horizontal slices at 1 to 2-, 2 to 3-, 3 to 4-km depth with zoom on the surveyed area. Labels outline low-V_p (a,b) and high-V_p (c) zones. The thin dashed line defines the AMT section. (e) Epicenters of the 1982–1984 earthquakes selected for the tomographic inversion. Epicenters are color coded based on hypocentral depth (1–2 km red, 2–3 km blue, 3–4 km dark blue). AMT = audiomagnetotelluric.

heterogeneities evidenced by our MT section. Nevertheless, information on V_p and V_p/V_s distributions is valuable to guide the interpretation of deeper, large-scale resistivity anomalies under Solfatara-Pisciarelli areas, especially in regard to the fluid physical state.

In the area investigated by our AMT survey, a very low V_p circular anomaly (V_p ~ 2.0 km/s) is centered underneath the Solfatara at 1- to 2-km depth (label *a* in Figure 11). Low V_p also characterizes the eastern sector of the Agnano depression (label *b* Figure 11), whereas an ordinary V_p around 3.2 km/s characterizes its western sector. The same velocity pattern is found between 2 to 3- and 3 to 4-km depth (Figures 11c and 11d, respectively). Two distinct low-V_p anomalies (V_p around 3.2–4.0 km/s) placed underneath the Solfatara (label *a*) and the eastern Agnano depression (label *b*) are separated by a narrow high-V_p zone (V_p around 4.4–4.8 km) that elongates N-S along the western margin of the Agnano depression (labels *c*). Earthquake relocations show that the 1982–1984 seismicity mostly clustered underneath the Solfatara (Figure 11e) just to the west of the N-S trending high-V_p boundary.

V_p, V_s, and V_p/V_s vertical profiles extracted from the 3D model were reported for several sites of the local seismic network. The W12 station (see Figures 11a and 11b in Vanorio et al., 2005) is located in the Solfatara area about 100 m away from the AMT section at about 1.1 km from its southwestern side. The

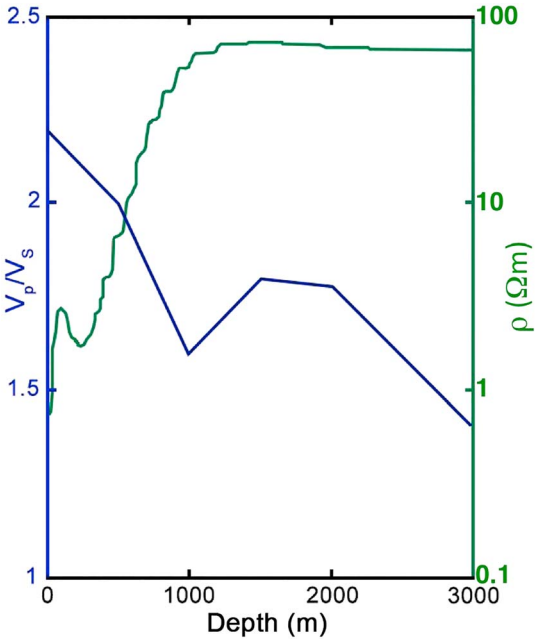

Figure 12. Comparison between the V_p/V_s ratio vertical profile (blue) at the seismometric station W12 (Vanorio et al., 2005) and the resistivity (in logarithmic scale) vertical profile (green) in the same location.

comparison with the correspondent resistivity vertical profile evidences a clear anticorrelation between V_p/V_s and resistivity (Figure 12). In particular, the V_p/V_s curve has a reversal trend (the value tends to decrease with depth) and a minimum in the V_p/V_s ratio at 1,000 m of depth

($V_p/V_s = 1.6$) corresponds to the maximum value in resistivity (around 80 Ω·m). It is worth to note that the core of the resistivity plume is localized just at 1,000 m bsl (Figure 10). Taken together, the spatial association of the high-resistivity plume with a very low V_p anomaly, the very low V_p/V_s, and the anticorrelation between resistivity and V_p/V_s points to the existence of a fractured, steam/gas-bearing zone just underneath the Solfatara crater and supports our interpretation of the high resistive plume as a prevailing gas-phase reservoir feeding the Solfatara-Pisciarelli shallow hydrothermal system. Overall, this finding is coherent with geochemical models of the hydrothermal system consisting of a deep-seated mixing zone and of a shallow zone interacting with each other (Caliro et al., 2007). Interaction with the shallow hydrothermal system should occur through fault-related interruptions of the clay-rich caps, while the Solfatara gas plume might be in turn fed by a deeper overpressured gas-bearing zone at supercritical condition that reasonably corresponds to the wide low-V_p/V_s layer identified at 4- to 5-km depth under the central caldera (Battaglia et al., 2008; Vanorio et al., 2005).

The deep conductive structure bounding the Solfatara plume to the east correlates to the N-S trending zone with ordinary to high V_p resolved from 1 to 2- to 3 to 4-km depth eastward from Solfatara (Figures 11b and 11d, label *c*). In this zone, the CF23 well drilled tuffs and volcanoclastic deposits encountered a relevant aquifer at 1,400 m of depth. Based on the CF23 well information, the adjacent conductive zone, with relatively high *P* wave velocities might represents water-bearing formations.

4.4. Comparison With Seismicity

The 1982–1984 and 2005-present unrest episodes are characterized by a differing earthquake distribution. During the 1982–1984 crisis, seismicity concentrated in the Solfatara area, whereas 2005–2016 seismicity avoids the zone of previous high seismic release and clusters eastward under the western margin of the Agnano depression (Figure 7). We remark that such a spatiotemporal earthquake distribution correlates with resistivity pattern along the AMT profile as follows (supporting information Figure S9). Seismic events belonging to the 1982–1984 unrest episode mainly cluster within the high-resistivity, very low V_p and low V_p/V_s zone (i.e., the plume in the depth range 0.5–2.5 km and between 0.5 and 1.5 km from the beginning of the AMT section), whereas the more recent seismicity concentrates inside the adjacent conductive zone. As explained in section 3.3, earthquake distribution, values of the Benioff's strain release, and the *b* value map (Figure 8) suggest that seismic release during 1982–1984 was driven by both the hydrothermal system and the stress concentration induced by intense ground deformation. Conversely, the hydrothermal system seems to play a primary role in inducing seismicity during the weaker unrest episode initiated in 2005. In particular, recent seismicity is mostly located outside the resistive gas plume, that is, at the margins of the pressurized gas reservoir, as expected in geothermal systems (Majer & McEvilly, 1979).

5. Discussion

The MT resistivity model has enlightened several new characteristics of the CFc central-eastern side. The resistivity image was compared with various geological and geophysical data to allow for a more general interpretation of the volcanological information. Here we discuss and present a new simple conceptual model that takes into account the most striking features revealed by our work (Figure 13).

The most remarkable finding from our inversion is the wide conductive zones, interpreted as clay caps, underneath the Solfatara-Pisciarelli area and the Agnano plain. As result of the present investigation we have estimated for the first time its extension and continuity in depth.

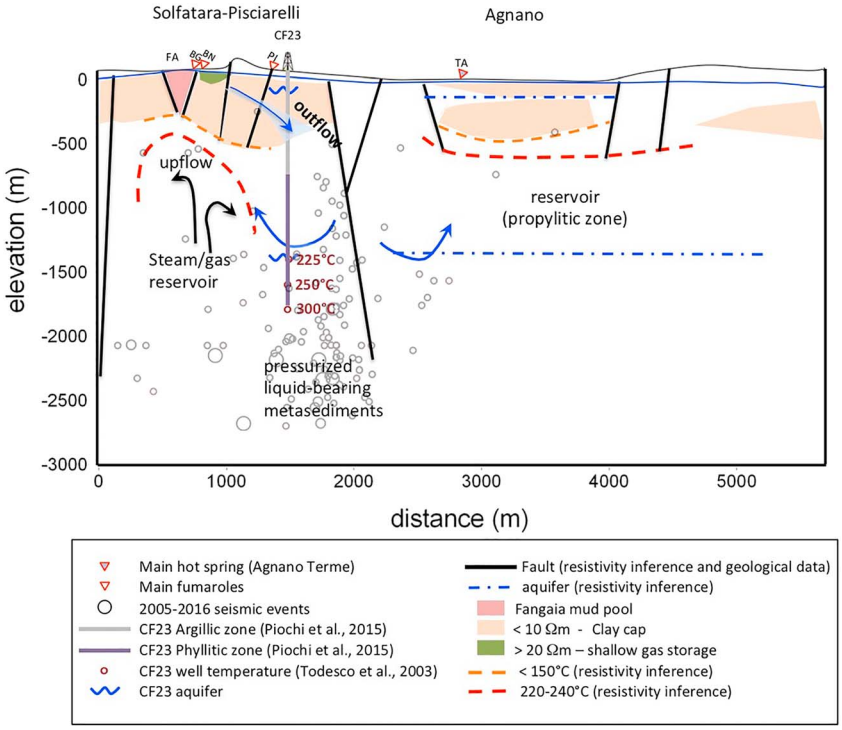

Figure 13. Conceptual model.

Both important processes of CO_2 soil diffuse degassing (Cardellini et al., 2017) and vigorous fumarolic vents occurrences (Aiuppa et al., 2013) characterize the Solfatara-Pisciarelli area. The total volcanic-hydrothermal CO_2 currently emitted into the atmosphere amounts to 2000–3000 tons per day, implying the involvement of several thousands of tons of steam most of which condensates in the subsoil, probably becoming the main factor contributing to the formation of the conductive clay cap. At a first glance, the high amount of gas daily released by the Solfatara-Pisciarelli fumaroles appears not compatible with the low permeability (generally 10^{-17} m^2) expected for clay. We will discuss about this apparent incongruity and investigate the role of the clay cap in the dynamics of the volcano-hydrothermal manifestation. As discussed in the previous section the interruptions in the conductive clay cap underneath the Solfatara-Pisciarelli sites interpreted as due to faults are spatially related to the main geochemical emissions (Figure 9). As reported by Mayer et al. (2016), laboratory experiments on samples from the Solfatara and Pisciarelli area reveal that increasing alteration and increasing permeability are expected with decreasing distance from the fumarole conduits. In particular, connected porosity and gas permeability increase from 26.6% to 61.3% and from 4.4×10^{-17} to 2.8×10^{-14} m^2 for Solfatara samples, as well as from 34.9% to 48.5% and from 2.2×10^{-16} to 1.8×10^{-15} m^2 for Pisciarelli samples. This suggests that permeability could increase up to 3 orders of magnitude within fractures discharging at the main vents, thus justifying the recovered degassing peaks. We further notice that just above the presumed cap interruptions (G2 in Figure 9c) and the maxima in the CO_2 flux (Figure 9b) the AMT model shows in the near surface of Solfatara a local increase of resistivity testifying for gas accumulation, in agreement with previous ERT shallow surveys (Byrdina et al., 2014; Gresse et al., 2017). Moreover, the inferred fault underneath Pisciarelli seems to be connected to the outflow zone (G3 in Figure 9c) that corresponds reasonably to condensates mixed with local meteoric recharge. This observation reconciles with the role of liquid water in the dynamic of the main fumarolic vent of the area that occasionally emits liquid and mud (Chiodini et al., 2011).

As for the increase of CO_2 diffuse degassing we advise that laboratory experiments have shown that the caprock seal capacity can be greatly reduced by cyclic flows of CO_2 brine and CO_2 gas (Andreani et al., 2008). The increasing permeability in the whole Solfatara-Pisciarelli area could be related to the complex interaction between H_2O-CO_2 magmatic gas mixtures in the hydrothermal system at subcritical

temperature and pressure conditions whose strong role with respect the CFc volcanic unrest was outlined in Chiodini et al. (2016).

This means that the existence of a fractured clay cap in the central-eastern sector of the CFc is a key character to be taken into account in any further modeling of the hydrogeothermal system.

At the eastern outer flank of the Solfatara crater the resistive vapor-dominated reservoir whose top is localized at about 500 m bsl under the conductive clayey zone should achieve temperatures of about 220–240° (Figure 13) as inferred by the widespread experience of resistivity behavior in high-temperature volcanic-associated geothermal systems. The hotter parts of the geothermal systems are characterized by a higher resistivity than what was observed in the adjacent hydrothermal alteration zone (Àrnason et al., 2010; Ussher et al., 2000). It is worth to note that gas geoindicators applied to the main Solfatara fumaroles return similar temperatures (210–240 °C, Chiodini et al., 2015).

The resistive plume matches the zone of high clusterization of earthquakes during the 1982–1984 unrest episode (supporting information Figure S9), whereas the 2005–2016 seismicity clusters at the eastern boundary of the 1982–1984 focal volume within the relative conductive zone detected in the depth range 0.5–2.5 km (Figure 10). Di Luccio et al. (2015) suggest that events distribution and fault geometries are consistent with a funnel-like structure within which brittle deformation have occurred. Also, to explain the lack of recent seismicity underlying the Solfatara, the authors speculate that this sector of the hydrothermal system could not represent a zone of brittle deformation at present. Rather, it might represent a very low rigidity zone linked to the formation of a dense network of fractures during the 1982–1984 crisis that was successively filled by high-temperature pressurized magmatic fluids.

Our finding of a fractured and high-temperature steam/gas-bearing reservoir just under the Solfatara reinforces previous inferences of Di Luccio et al. (2015). Based on our multidisciplinary conceptual model we propose that two main factors could contribute to the lack of seismicity underneath the Solfatara during the ongoing unrest episode: (i) increasing temperatures suggested by an evident thermal anomaly beneath the Solfatara (Chiodini et al., 2015; Gresse et al., 2017) could favor ductile deformation of the hydrothermal reservoir; (ii) enhancement of the reservoir fracture permeability induced, during the 1982–1984 unrest episode, by the sustained shallow seismicity clustered under the Solfatara area. Permeability enhancement would favor fluid flow within the Solfatara gas-bearing plume, as suggested by the increased rate of the Solfatara-Pisciarelli emissions (Chiodini et al., 2015). In addition, permeability enhancement would hamper the formation of overpressured zones within the gas-bearing reservoir that could induce seismicity during the ongoing unrest episode, as observed for fluid-driven swarm seismicity in other hydrothermal systems (Cox, 2016).

Conversely, recent seismicity to the east of the Solfatara could be induced by pore pressure increase within the relative conductive zone that might represent fractured liquid-bearing rocks, as inferred by the CF23 well and the V_p pattern of the LET models (Vanorio et al., 2005). In particular, Di Luccio et al. (2015) linked recent seismicity to NW-SE striking faults crossing the Pisciarelli degassing area. We remark that our AMT survey favors this interpretation because the lateral resistivity variations resolved in the shallow and deep parts of the section provide evidence of the continuity at depth of NW-SE active faults hypothesized previously by more authors (Isaia et al., 2015 among others, Figure 10).

In the Agnano plain, the CO_2 emission is orders of magnitude lower than that at Solfatara Pisciarelli (Figure 9b), as the measured CO_2 flux values are in the range of those due to soil biogenic sources. At Agnano, the main hydrothermal manifestation is the discharge of thermal water (springs and shallow wells) rather than gas emissions. The total water discharge (thermal component mixed with groundwaters) from the plain was measured in 2006 in ~ 140 L/s. Assuming a chlorine content of 15 g/L for the deep geothermal liquid (as the thermal liquid in CF23 geothermal well), we compute a discharge of ~ 9 L/s of NaCl pure geothermal component (of ~ 250 °C in origin) that variably mixes with shallow groundwaters. In the Agnano plain, higher pH values (almost neutral) differentiate the thermal water from the Solfatara-Pisciarelli area, where acid pH values (1.5–2.5) are recognized.

Summing up, both the resistive bodies located below the Solfatara-Pisciarelli and the Agnano plain (Figure 10) are expression of high-temperature alteration of the geothermal system that, however, have different characteristics. The resistive body with a prevailing vertical extension below the Solfatara-Pisciarelli is mainly caused by the presence of a highly active vapor-dominated reservoir generated by the episodic arrival

of CO_2-rich magmatic fluids (*S-P* vapor plume), while the resistive body below the Agnano plain with a prevailing horizontal extension is likely linked to the presence of a still hot reservoir. De Siena et al. (2010) interpreted a local attenuation anomaly detected in correspondence of the resistivity decrease at about 1,400 m as linked to the deep aquifer in the CF23 well that favors the upward circulation of hot nonmagmatic vapor. The existence of a still hot reservoir filled with nonmagmatic vapor also reconciles with the round shaped low-V_p anomaly detected under the Agnano depression (Figure 11).

The *S-P* vapor plume represents the main ascending way of magmatic gases. The physical modeling of hydrothermal circulation at CFc (i.e., Petrillo et al., 2013) has shown how the persistence in time of the vapor plume could have caused the development of convective cells of liquid in the surroundings. We speculate that Agnano could be the expression of the hot ascending portion mainly through conductive heat transfer of one of these convective cells.

6. Conclusions

The central-eastern sector of the CFc is an intensely studied and monitored active area. The presented resistivity model provides an image down to 3-km depth with an unprecedented high resolution with respect to previous geophysical models. Our resistivity model, analyzed in the light of new geochemical and seismicity observations, first reveals the typical characters of high- enthalpy geothermal systems, allowing to delineate a conceptual model (Figure 13). Among the most striking features revealed by this work there are the following.

1. A less permeable, conductive clay cap, whose variable thickness extends to a maximum of 500 m; it is locally interrupted in the Solfatara-Pisciarelli area by discontinuities characterized by increased permeability that are connected in surface to the main vents with the highest values of CO_2 flux.
2. Underneath the Solfatara, the base of the conductive clay cap is elevated and the top of a resistive vertical plume (*S-P* vapor plume) images the upflow zone of the geothermal system that extends eastward to the Pisciarelli area. This structure represents the main upraising pathway of magmatic gas from the deeper feeding reservoir. The resistive plume corresponds to a zone of high seismic release during the 1982–1984 unrest episode, whereas it has been almost aseismic in the following 30 years (cf. Figures 7a, 7b, and Figure S9).
3. A moderate resistive zone underneath the Pisciarelli area mirrors the topographic relief and separates the Solfatara from the Pisciarelli area. It is interpreted as a shallow zone where the outflow occurs deepening toward the region where most of the recent seismicity (last decade) is located.
4. Underneath the Agnano plain, the flat geometry of the resistive horizon above the clay zone and the prevalent discharges of thermal water suggest the prevalence of a liquid phase in the reservoir.

The main deeper resistivity features in the Solfatara-Pisciarelli district appear to be spatially connected to the post-1980 seismicity distribution (supporting information Figure S9). We argued that the fracture network induced by the intense and prolonged 1982–1984 seismic activity in this zone has further increased the permeability of this reservoir and then the fluid uprising from the feeding system. In this reservoir, a steam/gas phase is likely to occur according to the geochemical evidences as well as the observed resistivity maximum value ($> 100\ \Omega$ m). The outflow zone testifies the great water supply, both meteoric and from steam condensation, in this sector of the caldera that was characterized in the past by the occurrence of phreatic and phreatomagmatic eruptions (Isaia et al., 2015; Mayer et al., 2016). Recent seismic events cluster just in the foot of this zone marked by a lateral resistivity contrast that well matches the NW-SE striking fault crossing the Pisciarelli field. Furthermore, we can expect that the cooler water that permeates the rocks in the outflow zone coming in contact with the hotter gas/steam reservoir can play a role in the seismicity. The high local gradient of pressure, and even temperature, in this zone can make that part of the liquid suddenly change its state (flashing) producing steam, a consequent volume increase and new fractures opening that propagate along that fault (which acts as a tectonic control). In this view, the recent seismic events, mainly in swarm episodes, are linked to the combined action of preexisting tectonic lineaments and fluid interaction between the gas/steam reservoir and the outflow zone.

Moreover, the new insights into the geometry and properties of the hydrogeothermal system provided by our study are valuable for future thermodynamical modeling of the CFc and could be useful to better understand similar geodynamic environments.

Acknowledgments

This research is part of the MED-SUV project. MED-SUV has received funding from the European Union's Seventh Program for research, technological development, and demonstration under the call FP7 ENV.2012.6.4-2 and grant agreement 308665. The AMT equipment used in this study belongs to the Polo-Scientifico e Tecnologico of the University of Bari. This work is also supported by the Intervention cofinanced by the Fund of Development and Cohesion 2007–2013 - APQ Research Region of Apulia *Regional Program to support smart specialization and social and environmental sustainability—FutureInResearch*. We thank Tiziana Vanorio for providing the horizontal slices of the V_p tomographic model of the CFc. The data discussed in the manuscript are freely available at the link https://doi.org/10.17632/kn46886xvw.1 (DOI: 10.17632/kn46886xvw.1).

References

Acocella, V. (2010). Evaluating fracture patterns within a resurgent caldera: Campi Flegrei, Italy. *Bulletin of Volcanology*, *72*(5), 623–638. https://doi.org/10.1007/s00445-010-0347-x

Aiuppa, A., Tamburello, G., Di Napoli, R., Cardellini, C., Chiodini, G., Giudice, G., et al. (2013). First observations of the fumarolic gas output from a restless caldera: Implications for the current period of unrest (2005–2013) at Campi Flegrei. *Geochemistry, Geophysics, Geosystems*, *14*, 4153–4169. https://doi.org/10.1002/ggge.20261

Amoruso, A., Crescentini, L., & Sabbetta, I. (2014). Paired deformation sources of the Campi Flegrei caldera (Italy) required by recent (1980–2010) deformation history. *Journal of Geophysical Research: Solid Earth*, *119*, 858–879. https://doi.org/10.1002/2013JB010392

Anderson, E., Crosby, D., & Ussher, G. (2000). Bulls-eye!—Simple resistivity imaging to reliably locate the geothermal reservoir. Proc. World Geothermal Congress, Kyushu-Tohoku, Japan, pp. 909–914.

Andreani, M., Gouze, P., Luquot, L., & Jouanna, P. (2008). Changes in seal capacity of fractured claystone caprocks induced by dissolved and gaseous CO_2 seepage. *Geophysical Research Letters*, *35*, L14404. https://doi.org/10.1029/2008GL034467

Àrnason, K., Eysteinsson, H., & Hersir, G. P. (2010). Joint 1D inversion of TEM and MT data and 3D inversion of MT data in the Hengill area, SW Iceland. *Geothermics*, *39*(1), 13–34. https://doi.org/10.1016/j.geothermics.2010.01.002

Aster, R. C., & Meyer, R. P. (1988). Three-dimensional velocity structure and hypocenter distribution in the Campi Flegrei caldera, Italy. *Tectonophysics*, *149*(3-4), 195–218. https://doi.org/10.1016/0040-1951(88)90173-4

Battaglia, J., Zollo, A., Virieux, J., & Dello Iacono, D. (2008). Merging active and passive data sets in traveltime tomography: The case study of Campi Flegrei caldera southern Italy. *Geophysical Prospecting*, *56*(4), 555–573. https://doi.org/10.1111/j.1365-2478.2007.00687.x

Beamish, D., & Travassos, J. M. (1992). The use of the D+ solution in magnetotelluric interpretation. *Journal of Applied Geophysics*, *29*(1), 1–19. https://doi.org/10.1016/0926-9851(92)90009-A

Benioff, H. (1951). Earthquakes and rock creep: Part I. Creep characteristics of rocks and the origin of aftershocks. *Bulletin of the Seismological Society of America*, *41*(1), 31–62.

Berdichevsky, M. N. (1999). Marginal notes on magnetotellurics. *Surveys in Geophysics*, *20*(3/4), 341–375. https://doi.org/10.1023/A:1006645715819

Booker, J. R. (2014). The Magnetotelluric phase tensor: A critical review. *Surveys in Geophysics*, *35*(1), 7–40. https://doi.org/10.1007/s10712-013-9234-2

Bruno, P. G., Maraio, S., & Festa, G. (2017). The shallow structure of Solfatara volcano, Italy, revealed by dense, wide-aperture seismic profiling. *Scientific Reports*, *7*(1), 17386. https://doi.org/10.1038/s41598-017-17589-3

Bruno, P. G., Ricciardi, G. P., Petrillo, Z., Di Fiore, V., Troiano, A., & Chiodini, G. (2007). Geophysical and hydrogeological experiments from a shallow hydrothermal system at Solfatara Volcano, Campi Flegrei, Italy: Response to caldera unrest. *Journal of Geophysical Research*, *112*, B06201. https://doi.org/10.1029/2006JB004383

Byrdina, S., Vandemeulebrouck, J., Cardellini, C., Legaz, A., Camerlynck, C., Chiodini, G., et al. (2014). Relations between electrical resistivity, carbon dioxide flux, and self-potential in the shallow hydrothermal system of Solfatara (Phlegrean Fields, Italy). *Journal of Volcanology and Geothermal Research*, *283*, 172–182. https://doi.org/10.1016/j.jvolgeores.2014.07.010

Caldwell, T. G., Bibby, H. M., & Brown, C. (2004). The magnetotelluric phase tensor. *Geophysical Journal International*, *158*(2), 457–469. https://doi.org/10.1111/j.1365-246X.2004.02281.x

Caliro, S., Chiodini, G., Moretti, R., Avino, R., Granieri, D., Russo, M., & Fiebig, J. (2007). The origin of the fumaroles of La Solfatara (Campi Flegrei, South Italy). *Geochimica et Cosmochimica Acta*, *71*(12), 3040–3055. https://doi.org/10.1016/j.gca.2007.04.007

Caliro, S., Chiodini, G., & Paonita, A. (2014). Geochemical evidences of magma dynamics at Campi Flegrei (Italy). *Geochimica et Cosmochimica Acta*, *132*, 1–15. https://doi.org/10.1016/j.gca.2014.01.021

Calò, M., & Dorbath, C. (2013). Different behaviours of the seismic velocity field at Soultz-sous- Forêts revealed by 4-D seismic tomography: Case study of GPK3 and GPK2 injection tests. *Geophysical Journal International*, *194*(2), 1119–1137. https://doi.org/10.1093/gji/ggt153

Cardellini, C., Chiodini, G., & Frondini, F. (2003). Application of stochastic simulation to CO_2 flux from soil: Mapping and quantification of gas release. *Journal of Geophysical Research*, *108*(B9), 2425. https://doi.org/10.1029/2002JB002165

Cardellini, C., Chiodini, G., Frondini, F., Avino, R., Bagnato, E., Caliro, S., et al. (2017). Monitoring diffuse volcanic degassing during volcanic unrests: The case of Campi Flegrei (Italy). *Scientific Reports*, *7*(1), 6757. https://doi.org/10.1038/s41598-017-06941-2

Carlino, S., Somma, R., Troise, C., & De Natale, G. (2012). The geothermal exploration of Campanian volcanoes: Historical review and future development. *Renewable and Sustainable Energy Reviews*, *16*(1), 1004–1030. https://doi.org/10.1016/j.rser.2011.09.023

Chave, A. D., & Jones, A. G. (2012). *The magnetotelluric method: Theory and practice*. Cambridge: Cambridge University Press. https://doi.org/10.1017/CBO9781139020138

Chiodini, G., Avino, R., Caliro, S., & Minopoli, C. (2011). Temperature and pressure gs geoindicators at the Solfatara fumaroles (Campi Flegrei). *Annals of Geophysics*, *54*(2). https://doi.org/10.4401/ag-5002

Chiodini, G., Cioni, R., Guidi, M., Raco, B., & Marini, L. (1998). Soil CO_2 flux measurements in volcanic and geothermal areas. *Applied Geochemistry*, *13*(5), 543–552. https://doi.org/10.1016/S0883-2927(97)00076-0

Chiodini, G., Frondini, F., & Raco, B. (1996). Diffuse emission of CO_2 from the Fossa crater, Vulcano Island (Italy). *Bulletin of Volcanology*, *58*(1), 41–50. https://doi.org/10.1007/s004450050124

Chiodini, G., Paonita, A., Aiuppa, A., Costa, A., Caliro, S., De Martino, P., et al. (2016). Magmas near the critical degassing pressure drive volcanic unrest towards a critical state. *Nature Communications*, *7*(1), 13712. https://doi.org/10.1038/ncomms13712

Chiodini, G., Vandemeulebrouck, J., Caliro, S., D'Auria, L., De Martino, P., Mangiacapra, A., & Petrillo, Z. (2015). Evidence of thermal driven processes triggering the 2005–2014 unrest at Campi Flegrei caldera. *Earth and Planetary Science Letters*, *414*, 58–67. https://doi.org/10.1016/j.epsl.2015.01.012

Civetta, L., Orsi, G., Pappalardo, L., Fisher, R. V., Heiken, G., & Ort, M. (1997). Geochemical zoning, mingling, eruptive dynamics and depositional processes—The Campanian ignimbrite, Campi Flegrei caldera, Italy. *Journal of Volcanology and Geothermal Research*, *75*(3-4), 183–219. https://doi.org/10.1016/S0377-0273(96)00027-3

Cox, S. F. (2016). Injection-driven swarm seismicity and permeability enhancement: Implications for the dynamics of hydrothermal ore systems in high fluid-flux, overpressured faulting regimes. *Economic Geology*, *111*(3), 559–587. https://doi.org/10.2113/econgeo.111.3.559

Cumming, W. (2009). *Geothermal resource conceptual models using surface exploration data*. Proceedings of the 34th Workshop on Geothermal Reservoir Engineering, Stanford University, Stanford, CA.

D'Auria, L., Giudicepietro, F., Aquino, I., Borriello, G., Del Gaudio, C., Lo Bascio, D., et al. (2011). Repeated fluid-transfer episodes as a mechanism for the recent dynamics of Campi Flegrei caldera (1989–2010). *Journal of Geophysical Research*, *116*, B04313. https://doi.org/10.1029/2010JB007837

D'Auria, L., Pepe, S., Castaldo, R., Giudicepietro, F., Macedonio, G., Ricciolino, P., et al. (2015). Magma injection beneath the urban area of Naples: a new mechanism for the 2012–2013 volcanic unrest at Campi Flegrei caldera. *Scientific Reports*, *5*(1), 13100. https://doi.org/10.1038/srep13100

De Landro, G., Serlenga, V., Russo, G., Amoroso, O., Festa, G., Bruno, P. P., & Zollo, A. (2017). 3D ultra-high resolution seismic imaging of shallow Solfatara crater in Campi Flegrei (Italy): New insights on deep hydrothermal fluid circulation processes. *Scientific Reports*, *7*(1), 3412. https://doi.org/10.1038/s41598-017-03604-0

De Siena, L., Chiodini, G., Vilardo, G., Del Pezzo, E., Castellano, M., Colombelli, S., et al. (2017). Source and dynamics of a volcanic caldera unrest: Campi Flegrei, 1983–84. *Scientific Reports*, *7*(1), 8099. https://doi.org/10.1038/s41598-017-08192-7

de Lorenzo, S., Zollo, A., & Mongelli, F. (2001). Source parameters and 3-D attenuation structure from the inversion of microearthquake pulse width data: Qp imaging and inferences on the thermal state of the Campi Flegrei caldera. *Journal of Geophysical Research*, *106*(B8), 16265–16286. https://doi.org/10.1029/2000JB900462

De Siena, L., Del Pezzo, E., & Bianco, F. (2010). Seismic attenuation imaging of Campi Flegrei: Evidence of gas reservoirs, hydrothermal basins, and feeding systems. *Journal of Geophysical Research*, *115*, B09312. https://doi.org/10.1029/2009JB006938

de Vita, S., Orsi, G., Civetta, L., Carandente, A., D'Antonio, M., Di Cesare, T., et al. (1999). The Agnano–Monte Spina eruption (4.1 ka) in the resurgent, nested Campi Flegrei caldera (Italy). *Journal of Volcanology and Geothermal Research*, 269–301. https://doi.org/10.1016/S0377-0273(99)00039-6

Deutsch, C. V., & Journel, A. G. (1998). *GSLIB: Geostatistical software library and users guide*, *Applied Geostatistics Series* (Vol. 136). New York: Oxford University Press.

Di Luccio, F., Pino, N. A., Piscini, A., & Ventura, G. (2015). Significance of the 1982–2014 Campi Flegrei seismicity: Preexisting structures, hydrothermal processes, and hazard assessment. *Geophysical Research Letters*, *42*, 7498–7506. https://doi.org/10.1002/2015GL064962

Di Vito, M. A., Isaia, R., Orsi, G., Southon, J., de Vita, S., D'Antonio, M., et al. (1999). Volcanism and deformation since12,000 years at the Campi Flegrei caldera (Italy). *Journal of Volcanology and Geothermal Research*, *91*(2-4), 221–246. https://doi.org/10.1016/S0377-0273(99)00037-2

Farrel, J., Husen, S., & Smith, R. B. (2009). Earthquake swam and *b*-value characterization of the Yellowstone volcano-tectonic system. *Journal of Volcanology and Geothermal Research*, *188*(1-3), 260–276. https://doi.org/10.1016/j.jvolgeores.2009.08.008

Flóvenz, O.G., Spangerberg, E., Kulenkampff, J., Árnason, K., Karlsdottir, R., & Huenges, E. (2005). *The role of electrical interface conduction in geothermal exploration*, Proceedings of the World Geothermal Congress (pp. 1–7), Antalya, Turkey.

García-Hernández, R., D'Auria, L., Barrancos, J., & Padilla, G. D. (2018). Multiscale spatio-temporal determination of the b-value. Geophysical Research Abstracts Vol. 20, EGU2018-3393-1.

Giberti, G., Yven, B., Zamora, M., & Vanorio, T. (2006). Database of laboratory measured data on physical properties of rocks at Campi Flegrei volcanic area (Italy). In A. Zollo, P. Capuano, & M. Corciulo (Eds.), *Geophysical exploration of the Campi Flegrei (Southern Italy) caldera interiors: Data, methods and results* (pp. 179–192). Naples: Doppia Voce. ISBN: 978-88-89972-04-5.

Gresse, M., Vandemeulebrouck, J., Byrdina, S., Chiodini, G., Revil, A., Johnson, T. C., et al. (2017). Three-dimensional electrical resistivity tomography of the Solfatara crater (Italy): Implication for the multiphase flow structure of the shallow hydrothermal system. *Journal of Geophysical Research: Solid Earth*, *122*, 8749–8768. https://doi.org/10.1002/2017JB014389

Guidoboni, E., & Ciuccarelli, C. (2010). The Campi Flegrei caldera: Historical revision and new data on seismic crises, bradyseisms, the Monte Nuovo eruption and ensuing earthquakes (twelfth century 1582 AD). *Bulletin of Volcanology*, *73*(6), 655–677. https://doi.org/10.1007/s00445-010-0430-3

Husen, S., Smith, R. B., & Waite, G. P. (2004). Evidence for gas and magmatic sources beneath the Yellowstone volcanic field from seismic tomographic imaging. *Journal of Volcanology and Geothermal Research*, *131*(3-4), 397–410. https://doi.org/10.1016/S0377-0273(03)00416-5

Isaia, R., Vitale, S., Di Giuseppe, M. G., Iannuzzi, E., Tramparulo, F. D. A., & Troiano, A. (2015). Stratigraphy, structure, and volcano-tectonic evolution of Solfatara maar–diatreme (Campi Flegrei, Italy). *Geological Society of America Bulletin*, B31183-1.

Johnston, J. M., Pellerin, L., & Hohmann, G. W. (1992). Evaluation of electromagnetic methods for geothermal reservoir detection. *Geothermal Resource Council Transactions*, *16*, 241–245.

Jones, A. G. (1983). The problem of current channelling: A critical review. *Geophysical Surveys*, *6*(1-2), 79–122. https://doi.org/10.1007/BF01453996

Julian, B. R., Foulger, G. R., Monastero, F. C., & Bjornstad, S. (2010). Imaging hydraulic fractures in a geothermal reservoir. *Geophysical Research Letters*, *37*, L07305. https://doi.org/10.1029/2009GL040933

Kaven, J. O., Hickman, S. H., & Davatzes N. C. (2014). *Micro-seismicity and seismic moment release within the Coso Geothermal Field, California*. Proceedings of the 39th Workshop on Geothermal Reservoir Engineering (p. 10), Stanford University, Stanford, Calif.

Komori, S., Kagiyama, T., Takakura, S., Ohsawa, S., Mimura, M., & Mogi, T. (2013). Effect of the hydrothermal alteration on the surface conductivity of rock matrix: Comparative study between relatively-high and low temperature hydrothermal systems. *Journal of Volcanology and Geothermal Research*, *264*(2013), 164–171. https://doi.org/10.1016/j.jvolgeores.2013.08.009

Ledo, J. (2005). 2-D versus 3-D magnetotelluric data interpretation. *Surveys in Geophysics*, *26*(5), 511–543. https://doi.org/10.1007/s10712-005-1757-8

Majer, E. L., & McEvilly, T. V. (1979). Seismological investigations at The Geysers geothermal field. *Geophysics*, *44*(2), 246–269. https://doi.org/10.1190/1.1440965

Martí, A., Queralt, P., & Roca, E. (2004). Geoelectric dimensionality in complex geologic areas: Application to the Spanish Betic Chain. *Geophysical Journal International*, *157*(3), 961–974. https://doi.org/10.1111/j.1365-246X.2004.02273.x

Mayer, K., Scheu, B., Montanaro, C., Yilmaz, T. I., Isaia, R., Aßbichler, D., & Dingwell, D. B. (2016). Hydrothermal alteration of surficial rocks at Solfatara (Campi Flegrei): Petrophysical properties and implications for phreatic eruption processes. *Journal of Volcanology and Geothermal Research*, *320*, 128–143. https://doi.org/10.1016/j.jvolgeores.2016.04.020

Miensopust, M. P., Queralt, P., Jones, A. G., & the 3D MT modellers (2013). Magnetotelluric 3-D inversion—A review of two successful workshops on forward and inversion code testing and comparison. *Geophysical Journal International*, *193*(3), 1216–1238. https://doi.org/10.1093/gji/ggt066

Munoz, G. (2014). Exploring for geothermal resources with electromagnetic methods. *Surveys in Geophysics*, *35*(1), 101–122. https://doi.org/10.1007/s10712-013-9236-0

Nolasco, R., Tarits, P., Filloux, J., & Chave, A. (1998). Magnetotelluric imaging of the Society Islands hotspot. *Journal of Geophysical Research*, *103*(B12), 30287–30309. https://doi.org/10.1029/98JB02129

Ogata, Y., & Katsura, K. (1993). Analysis of temporal and spatial heterogeneity of magnitude frequency distribution inferred from earthquake catalogues. *Geophysical Journal International*, *113*(3), 727–738. https://doi.org/10.1111/j.1365-246X.1993.tb04663.x

Ogawa, Y. (2002). On two-dimensional modeling of magnetotelluric field data. *Surveys in Geophysics*, *23*(2/3), 251–273. https://doi.org/10.1023/A:1015021006018

Orsi, G., de Vita, S., & Di Vito, M. (1996). The restless, resurgent Campi Flegrei nested caldera (Italy): Constraints on its evolution and configuration. *Journal of Volcanology and Geothermal Research*, *74*(3-4), 179–214. https://doi.org/10.1016/S0377-0273(96)00063-7

Parascandola, A. (1983). *I Fenomeni Bradisismici del Serapeo di Pozzuoli* (p. 120). Naples, Italy: Guida Editore.

Petrillo, Z., Chiodini, G., Mangiacapra, A., Caliro, S., Capuano, P., Russo, G., et al. (2013). Defining a 3D physical model for the hydrothermal circulation at Campi Flegrei caldera (Italy). *Journal of Volcanology and Geothermal Research*, *264*, 172–182. https://doi.org/10.1016/j.jvolgeores.2013.08.008

Piochi, M., Kilburn, C. R. J., Di Vito, M. A., Mormone, A., Tramelli, A., Troise, C., & De Natale, G. (2014). The volcanic and geothermally active Campi Flegrei caldera: An integrated multidisciplinary image of its buried structure. *International Journal of Earth Sciences*, *103*(2), 401–421. https://doi.org/10.1007/s00531-013-0972-7

Piochi, M., Mormone, A., Balassone, G., Strauss, H., Troise, C., & De Natale, G. (2015). Native sulfur, sulfates and sulfides from the active Campi Flegrei volcano (southern Italy): Genetic environments and degassing dynamics revealed by mineralogy and isotope geochemistry. *Journal of Volcanology and Geothermal Research*, *304*, 180–193. https://doi.org/10.1016/j.jvolgeores.2015.08.017

Rodi, W., & Mackie, R. L. (2001). Nonlinear conjugate gradients algorithm for 2-D magnetotelluric inversion. *Geophysics*, *66*(1), 174–187. https://doi.org/10.1190/1.1444893

Rodriguez, F., Pérez, N. M., Padrón, E., Melián, G., Piña-Varas, P., Dionis, S., et al. (2015). Surface geochemical and geophysical studies for geothermal exploration at the southern volcanic rift zone of Tenerife, Canary Islands, Spain. *Geothermics*, *55*, 195–206. https://doi.org/10.1016/j.geothermics.2015.02.007

Romano, G., Balasco, M., Lapenna, V., Siniscalchi, A., Telesca, L., & Tripaldi, S. (2014). On the sensitivity of long-term magnetotelluric monitoring in Southern Italy and source-dependent robust single station transfer function variability. *Geophysical Journal International*, *197*(3), 1425–1441. https://doi.org/10.1093/gji/ggu083

Rosi, M., & Sbrana, A. (1987). *Phlegraean fields*. Rome: Quad. de La Ric. Sci., CNR Ed.

Rouwet, D., Sandri, L., Marzocchi, W., Gottsmann, J., Selva, J., Tonini, R., & Papale, P. (2014). Recognizing and tracking volcanic hazards related to non-magmatic unrest: a review. *Journal of Applied Volcanology*, *3*(17). https://doi.org/10.1186/s13617-014-0017-3

Simpson, F., & Bahr, K. (2005). *Practical magnetotellurics*. Cambridge: Cambridge University Press. https://doi.org/10.1017/CBO9780511614095

Spichak, V., & Manzella, A. (2009). Electromagnetic sounding of geothermal zones. *Journal of Applied Geophysics*, *68*(4), 459–478. https://doi.org/10.1016/j.jappgeo.2008.05.007

Sternberg, B. K., Washburne, J. C., & Pellerin, L. (1988). Correction for the static shift in magnetotellurics using transient electromagnetic soundings. *Geophysics*, *53*, 1459–1468. https://doi.org/10.1190/1.1442426

Tietze, K., & Ritter, O. (2013). Three-dimensional magnetotelluric inversion in practice-the electrical conductivity structure of the San Andreas fault in central California. *Geophysical Journal International*, *195*(1), 130–147. https://doi.org/10.1093/gji/ggt234

Tikhonov, A. N., & Arsenin, V. Y. (1977). *Solutions of ill-posed problems*. Washington, D.C.: V.H. Winston and Sons.

Todesco, M., Chiodini, G., & Macedonio, G. (2003). Monitoring and modeling hydrothermal fluid emission at La Solfatara (Phlegrean Fields, Italy): An interdisciplinary approach to the study of diffuse degassing. *Journal of Volcanology and Geothermal Research*, *125*(1-2), 57–79. https://doi.org/10.1016/S0377-0273(03)00089-1

Tramelli, A., Del Pezzo, E., Bianco, F., & Boschi, E. (2006). 3D scattering image of the Campi Flegrei caldera (Southern Italy): New hints on the position of the old caldera rim. *Physics of the Earth and Planetary Interiors*, *155*(3-4), 269–280. https://doi.org/10.1016/j.pepi.2005.12.009

Tripaldi, S., Siniscalchi, A., & Spitzer, K. (2010). A method to determine the magnetotelluric static shift from DC resistivity measurements in practice. *Geophysics*, *75*(1), F23–F32. https://doi.org/10.1190/1.3280290

Troiano, A., Di Giuseppe, M. G., Patella, D., Troise, C., & De Natale, G. (2014). Electromagnetic outline of the Solfatara–Pisciarelli hydrothermal system, Campi Flegrei (Southern Italy). *Journal of Volcanology and Geothermal Research*, *277*, 9–21. https://doi.org/10.1016/j.jvolgeores.2014.03.005

Ussher, G., Harvey, C., Johnston, R., & Anderson, E. (2000). *Understanding the resistivities observed in geothermal systems*. Proceedings of the World Geothermal Congress (pp. 1915–1920), Kyushu-Tohoku, Japan.

Vanorio, T., & Kanitpanyacharoen, W. (2015). Rock physics of fibrous rocks akin to Roman concrete explains uplifts at Campi Flegrei caldera. *Science*, *349*(6248), 617–621. https://doi.org/10.1126/science.aab1292

Vanorio, T., Virieux, J., Capuano, P., & Russo, G. (2005). Three-dimensional seismic tomography from *P* wave and *S* wave microearthquake travel times and rock physics characterization of the Campi Flegrei caldera. *Journal of Geophysical Research*, *110*, B03201. https://doi.org/10.1029/2004JB003102

Vaselli, O., Tassi, F., Tedesco, D., Poreda, J. R., & Caprai, A. (2011). Submarine and inland gas discharges from the Campi Flegrei (southern Italy) and the Pozzuoli Bay: Geochemical clues for a common hydrothermal-magmatic source. *Procedia Earth and Planetary Science*, *4*, 57–73.

Vilardo, G., Isaia, R., Ventura, G., De Martino, P., & Terranova, C. (2010). InSAR permanent scatter analysis reveals fault re-activation during inflation and deflation episodes at Campi Flegrei caldera. *Remote Sensing of Environment*, *114*(10), 2373–2383. https://doi.org/10.1016/j.rse.2010.05.014

Wang, Z. W., & Nur, A. (1989). Effect of CO_2 flooding on wave velocities in rocks and hydrocarbons. *Society of Petroleum Engineers Reservoir Engineering*, *3*, 429–439.

Wannamaker, P. E., Hohmann, G. W., & Ward, S. H. (1984). Magnetotelluric responses of three-dimensional bodies in layered Earths. *Geophysics*, *49*(9), 1517–1533. https://doi.org/10.1190/1.1441777

Weaver, J. T., Agarwal, A. K., & Lilley, F. E. M. (2000). Characterisation of the magnetotelluric tensor in terms of its invariants. *Geophysical Journal International*, *141*(2), 321–336. https://doi.org/10.1046/j.1365-246x.2000.00089.x

Zollo, A., Maercklin, N., Vassallo, M., Dello Iacono, D., Virieux, J., & Gasparini, P. (2008). Seismic reflections reveal a massive melt layer feeding Campi Flegrei caldera. *Geophysical Research Letters*, *35*, L12306. https://doi.org/10.1029/2008GL034242